1 *Full paper*

2 New insights into the mechanisms of plant isotope fractionation from combined analysis

3 of intramolecular ^{13}C and deuterium abundances in *Pinus nigra* tree-ring glucose

4 Thomas Wieloch[1,2,*], Meisha Holloway-Phillips[3], Jun Yu[4], Totte Niittylä[1]

5

6 [1] Department of Forest Genetics and Plant Physiology, Swedish University of Agricultural Sciences, Umeå

7 Plant Science Centre, 90183 Umeå, Sweden

8 [2] Division of Geological and Planetary Sciences, California Institute of Technology, 91125 Pasadena, USA

9 [3] Research Unit of Forest Dynamics, Swiss Federal Institute for Forest, Snow and Landscape Research

10 WSL, 8903 Birmendsorf, Switzerland

11 [4] Department of Mathematics and Mathematical Statistics, Umeå University, 90187 Umeå, Sweden

12 * Corresponding author, Thomas Wieloch, thomas.wieloch@slu.se

13

14 **Keywords:** carbon stable isotopes, hydrogen stable isotopes, intramolecular isotope analysis, isotope

15 fractionation mechanisms, leaf water status, plant-environment interactions, stem water status, tree rings

16

17 6449 words (Introduction, Material and Methods, Results, Discussion), 6 Figures (colour), 7 Tables,

18 Supporting Information including 3 Notes, 6 Tables, and 1 Figure

19

Author	Email address	ORCID
Thomas Wieloch	thomas.wieloch@slu.se	0000-0001-9162-2291
Meisha Holloway-Phillips	meisha.holloway@wsl.ch	0000-0002-8353-3536
Jun Yu	jun.yu@umu.se	0000-0001-5673-620X
Totte Niittylä	totte.niittyla@slu.se	0000-0001-8029-1503

20

Summary

21   - Understanding isotope fractionation mechanisms is fundamental for analyses of plant ecophysiology and

23   paleoclimate based on tree-ring isotope data.

24

25   - To gain new insights into isotope fractionation, we analysed intramolecular ^{13}C discrimination in tree-ring

26   glucose (Δ_i', i = C-1 to C-6) and metabolic deuterium fractionation at H^1 and H^2 (ε_{met}) combinedly. This dual-

27   isotope approach was used for isotope-signal deconvolution.

28

29   - We found evidence for metabolic processes affecting Δ_1' and Δ_3' which respond to air vapour pressure

30   deficit (*VPD*), and processes affecting Δ_1', Δ_2', and ε_{met} which respond to precipitation but not *VPD*. These

31   relationships exhibit change points dividing a period of homeostasis (1961-1980) from a period of metabolic

32   adjustment (1983-1995). Homeostasis may result from sufficient groundwater availability. Additionally, we

33   found Δ_5' and Δ_6' relationships with radiation and temperature which are temporally stable and consistent

34   with previously proposed isotope fractionation mechanisms.

35

36   - Based on the multitude of climate covariables, intramolecular carbon isotope analysis has a remarkable

37   potential for climate reconstruction. While isotope fractionation beyond leaves is currently considered to be

38   constant, we propose significant parts of the carbon and hydrogen isotope variation in tree-ring glucose

39   originate in stems (precipitation-dependent signals). As basis for follow-up studies, we propose

40   mechanisms introducing Δ_1', Δ_2', Δ_3', and ε_{met} variability.

41

42   **Introduction**

43   Analysis of the systematic ^{13}C/^{12}C variation (commonly termed "^{13}C signal"; abbreviations in Table 1) across

44   tree-ring series is widely used to study past climate conditions, plant-environment interactions, and

45   physiological traits such as leaf water-use efficiency (CO_2 uptake relative to H_2O loss) (Leavitt & Roden,

46   2022). Signals found at the whole-tissue or whole-molecule level (Fig. 1A, top and middle) are commonly

47   interpreted based on a simplified mechanistic model of ^{13}C discrimination, Δ (denoting ^{13}C/^{12}C variation

48   caused by physiological processes) (Farquhar *et al.*, 1982). This model considers isotope effects of CO_2

49   diffusion from ambient air into intercellular air spaces (Craig, 1953) and CO_2 assimilation by rubisco

50   (Roeske & O'Leary, 1984) and phospho*enol*pyruvate carboxylase (PEPC; Fig. 2) (Farquhar, 1983;

51   Farquhar & Richards, 1984). Manifestation of these effects as ^{13}C discrimination depends on the ratio of

52   intercellular-to-ambient CO_2 partial pressure (p_i/p_a) (Farquhar *et al.*, 1982), and a highly significant positive

53   relationship between p_i/p_a and leaf Δ was confirmed experimentally (Evans *et al.*, 1986). Environmental

54   parameters influence p_i/p_a and thus leaf Δ (Evans *et al.*, 1986) by affecting the stomatal aperture and CO_2

55   assimilation. For instance, in response to drought, isohydric plant species such as *Pinus nigra* (studied

56   here) close their stomata (McDowell *et al.*, 2008). This can be expected to decrease p_i/p_a and leaf Δ

57   (Farquhar *et al.*, 1982; Evans *et al.*, 1986).

58

59   Isotope fractionation by metabolic processes downstream of CO_2 assimilation is complex (Hobbie &

60   Werner, 2004), incompletely understood (Badeck *et al.*, 2005; Cernusak *et al.*, 2009) and has yet to be

61   adequately integrated into ^{13}C-discrimination models (Ubierna *et al.*, 2022). Specifically, the simple [13]C

62   discrimination model described above requires multiple adaptations to enable correct interpretation of the

63   [13]C composition of tree-ring glucose (studied here). For instance, we recently argued that incorporation of

64   carbon assimilated by PEPC into tree-ring glucose is negligible because leaves lack a high-flux pathway

65   shuttling this carbon into glucose metabolism (Fig. 2) (Wieloch *et al.*, 2022c). Therefore, all carbon in tree-

66   ring glucose proposedly derives from rubisco-assimilated CO_2. Rubisco catalyses the addition of CO_2 to

67   ribulose 1,5-bisphosphate (RuBP). Since this reaction is essentially the sole carbon source of glucose, [13]C

68   discrimination accompanying CO_2 diffusion and subsequent rubisco CO_2 assimilation (denoted diffusion-

69   rubisco discrimination) is expected to affect all glucose carbon positions equally (Wieloch *et al.*, 2018,

70   2022c).

71

72   Moreover, we recently measured Δ intramolecularly at all six carbon positions, *i*, of glucose (Fig. 1A, bottom)

73   extracted across an annually resolved tree-ring series of *Pinus nigra* (Wieloch *et al.*, 2018). The resultant

74   Δ_i' dataset comprises 6*31 values (study period: 1961 to 1995; four years missing: 1977, 1978, 1981, 1982)

75   which were corrected for ^{13}C signal redistribution by heterotrophic triose phosphate cycling (indicated by

76   prime, Supporting Information Notes S1). We found that, at least, four ^{13}C signals contribute to the

77   interannual ^{13}C/^{12}C variability in tree-ring glucose (Fig. 1B) and proposed the following theories on

78   underlying mechanisms.

79

80   We initially proposed the diffusion-rubisco signal is preserved at C-1 to C-3 (Figs. 1B and 2) (Wieloch *et al.*,

81   2018); although this view is modified here. Additionally, C-1 and C-2 are thought to carry ^{13}C signals due

82   to fractionation at phosphoglucose isomerase (PGI has carbon isotope effects at both C-1 and C-2) and

83   glucose-6-phosphate dehydrogenase (G6PD has a carbon isotope effect at C-1) (Wieloch *et al.*, 2018,

84   2022a). Two leaf-level mechanisms of signal introduction were proposed. First, with decreasing carbon

85   assimilation, the PGI reaction in chloroplasts moves from being on the side of fructose 6-phosphate (F6P)

86   towards equilibrium (Fig. 2) (Dietz, 1985). This shift is expected to cause ^{13}C enrichments at C-1 and C-2

87   of glucose 6-phosphate (G6P) and its derivatives starch and tree-ring glucose (Table 2) (Wieloch *et al.*,

88   2018). Moreover, shifts towards PGI equilibrium are associated with G6P increases (Dietz, 1985).

89   Increasing G6P is thought to cause G6PD activation and thus increasing flux through the oxidative pentose

90   phosphate pathway (OPPP) in chloroplasts (Cossar *et al.*, 1984; Sharkey & Weise, 2016; Preiser *et al.*,

91   2019) resulting in additional ^{13}C enrichment at C-1 of G6P and its derivatives (Wieloch *et al.*, 2022a).

92   Hydrogen isotope evidence consistent with these proposed metabolic shifts was reported recently (Wieloch

93   *et al.*, 2022a). Second, the PGI reaction in chloroplasts is usually displaced from equilibrium on the side of

94   F6P whereas the PGI reaction in the cytosol is closer to or in equilibrium (Dietz, 1985; Gerhardt *et al.*, 1987;

95   Leidreiter *et al.*, 1995; Schleucher *et al.*, 1999; Szecowka *et al.*, 2013). This is expected to result in $^{13}C/^{12}C$

96   differences between starch and sucrose at both hexose C-1 and C-2 (Table 2) (Wieloch *et al.*, 2022b). By

97   extension, changes in the relative contribution of starch to the biosynthesis of tree-ring glucose is expected

98   to contribute to the ^{13}C signals at C-1 and C-2.

99

100   In addition to ^{13}C signals at C-1 and C-2, tree-ring glucose samples discussed here carry deuterium signals

101   caused by metabolic processes at H^1 and H^2. These signals are strongly correlated and were approximated

102   as

103

$$\varepsilon_{\mathrm{met}} = \frac{(D_1 + D_2)/2}{(D_3 + D_4 + D_5 + D_{6S} + D_{6R})/5} - 1 \tag{1}$$

104

105   where D_i denotes relative deuterium abundances at individual H-C positions (Wieloch *et al.*, 2022a,b).

106   Variability of $\varepsilon_{\mathrm{met}}$ pertaining to glucose H^1 and H^2 was attributed to isotope effects of G6PD ($k_{\mathrm{H}}/k_{\mathrm{D}} = 2.97$)

107   (Hermes *et al.*, 1982) and PGI (Table 2) (Rose & O'Connell, 1961; Wieloch *et al.*, 2022a,b), respectively.

108   Proposedly, G6PD and PGI-dependent metabolic processes in both leaves and tree rings may contribute

109   to $\varepsilon_{\mathrm{met}}$ signal introduction (Wieloch *et al.*, 2022b). Interestingly, Wacker (2022) recently reported that the

110   commonly observed whole-molecule deuterium depletion of leaf starch which derives from deuterium

111   depletion at starch glucose H^2 (Schleucher *et al.*, 1999; Wieloch *et al.*, 2022a) is not detectable in nocturnal

112   sucrose. Proposedly, this depletion is either washed out at the level of cytosolic PGI or masked either by

113   the vacuolar sucrose pool or deuterium enrichments at other sucrose hydrogen positions. Washout would

114   imply that any $\varepsilon_{\mathrm{met}}$ signal present at leaf-level G6P H^2 is lost to the medium. In this case, the $\varepsilon_{\mathrm{met}}$ signal at

115   tree-ring glucose H^2 may originate outside of leaves.

116

117   At tree-ring glucose C-4 (Fig. 1B), the diffusion-rubisco ^{13}C signal is thought to be absent due to

118   counteracting fractionation by leaf-cytosolic glyceraldehyde-3-phosphate dehydrogenases (GAPDH; Fig.

119   2) (Wieloch *et al.*, 2021). Signal removal may involve both changes in 3-phosphoglycerate (PGA) flux into

120   downstream metabolism including the tricarboxylic acid cycle (TCAC) relative to flux into tree-ring glucose

121   and changes of flux through the cytosolic oxidation-reduction cycle (Wieloch, 2021; Wieloch *et al.*, 2021).

122

123   The ^{13}C signal at C-5 and C-6 (Fig. 1B) is thought to derive from the postulated (but not yet measured)

124   isotope effects of leaf-level enzymes that modify the carbon double bond in phospho*enol*pyruvate (PEP,

125   Fig. 2) (Wieloch *et al.*, 2022c). This includes enolase, pyruvate kinase (PK), PEPC, and 3-deoxy-D-*arabino*-

126   heptulosonate-7-phosphate synthase (DAHPS), the first enzyme of the shikimate pathway. Breaking the

127   double bond in PEP is thought to proceed faster when ^{12}C instead of ^{13}C forms this bond (Wieloch *et al.*,

128   2022c). Consequently, increasing relative flux into metabolism downstream of PEP is thought to ^{13}C enrich

129   remaining PEP at the double-bond carbons and their derivatives including glucose C-5 and C-6 (Wieloch

130   *et al.*, 2022c). For example, O_3 causes downregulation of rubisco, upregulation of PEPC, and DAHPS

4

131   expression (Dizengremel, 2001; Janzik *et al.*, 2005; Betz *et al.*, 2009). This is expected to cause increasing

132   relative flux into metabolism downstream of PEP (Wieloch *et al.*, 2022c). Accordingly, we previously found

133   a negative relationship between reconstructed tropospheric O_3 concentration and tree-ring glucose $\Delta_{5\text{-}6}'$

134   (arithmetic average of Δ_5' and Δ_6', Table 1) (Wieloch *et al.*, 2022c).

135

136   By contrast, the diffusion-rubisco signal is not evident at C-5 and C-6 (Wieloch *et al.*, 2022c). This was

137   explained (*inter alia*) by interaction between photorespiration and the TCAC (Fig. 2, Wieloch *et al.*, 2022c).

138   Photorespiration increases with drought which results in increasing supply of mitochondrial NADH via the

139   glycine decarboxylase complex. Since this NADH can feed oxidative phosphorylation, NADH and $FADH_2$

140   supply by the TCAC which requires injection of PEP into the TCAC via PK and PEPC may be reduced. This

141   should result in $\Delta_{5\text{-}6}'$ increases counteracting drought-induced decreases in diffusion-rubisco discrimination

142   (see above).

143

144   The theories of isotope signal introduction outlined above require further testing. They derive from separate

145   analyses of either the Δ_i' or deuterium dataset. However, some reactions exhibit both carbon and hydrogen

146   isotope effects (e.g., G6PD at G6P C-1 and H^1; PGI at G6P C-1, C-2, and H^2 but not H^1) and should

147   therefore introduce intercorrelated ^{13}C and deuterium signals (suggested terminology: hydro-carbon isotope

148   signals and hydro-carbon isotope fractionation). Combined analysis of intramolecular ^{13}C and deuterium

149   data can, in principle, help to separate those signals from signals introduced by reactions which merely

150   exhibit either carbon or hydrogen isotope effects. Therefore, we here studied the relationships between Δ_i'

151   and ε_{met} and their dependence on environmental parameters. Based on our results, we critically examine

152   and revise existing isotope theory and provide new insights into a central open question—whether carbon

153   and hydrogen isotope variability across tree rings derives from leaf-level processes only (as supported by

154   current evidence) or whether processes in the stem contribute as well.

155

156   **Material and Methods**

157   The Δ_i' and ε_{met} datasets reanalysed here are described in Wieloch *et al.* (2018, 2022b) and in Notes S1.

158   Data of relative humidity, precipitation (*PRE*), global radiation (*RAD*), sunshine duration (*SD*), and air

159   temperature (*TMP*) are from the climate station Hohe Warte (Vienna, Austria, 48.23° N, 16.35° E, 198 m

160   AMSL) (Klein Tank *et al.*, 2002). Air vapour pressure deficit (*VPD*) was calculated following published

161   procedures (Abtew & Melesse, 2013). Data of the standardised precipitation-evapotranspiration index

162   (*SPEI_i*) calculated for integrated periods of i = 1, 3, 6, 8, 12, 16, 24, 36, 48 months were obtained for 48.25°

163   N, 16.25° E (Fan & van den Dool, 2004; Beguería *et al.*, 2010). The *SPEI* is a multi-scalar drought index

164   approximating soil moisture variability when calculated for short timescales and groundwater variability

165   when calculated for long timescales (Vicente-Serrano *et al.*, 2010). The *RAD* series starts in 1964 while all

166   other climate series start in 1961. Horizontal distances between the tree site and the climate station and

5

167   grid point are < 15 km. Vertical offsets are small. Hence, climate data and site conditions are expected to

168   be in good agreement. Analytical procedures are described in Notes S1.

169

170   **Results**

171   *Hydro-carbon isotope signals at tree-ring glucose HC-1 and HC-2*

172   Tree-ring glucose of our *Pinus nigra* samples exhibits strongly correlated hydrogen isotope signals at H^1

173   and H^2 (Wieloch *et al.*, 2022b). These signals occur only after crossing a change point in 1980. Isotope-

174   environment-relationship analyses indicated that the trees had likely access to groundwater before 1980

175   which prevented changes of the processes introducing these isotope signals. We proposed the signals

176   derive from the hydrogen isotope effects of G6PD ($k_H/k_D = 2.97$) (Hermes *et al.*, 1982) and PGI (Table 2)

177   (Rose & O'Connell, 1961; Wieloch *et al.*, 2022a) in autotrophic and/or heterotrophic tissue (Fig. 2;

178   'Introduction') (Wieloch *et al.*, 2022a,b). If this proposal is correct then there should be related signals in Δ_1'

179   and Δ_2' due to the carbon isotope effects of G6PD affecting C-1 ($k_{^{12}C}/k_{^{13}C} = 1.0165$) (Hermes *et al.*, 1982)

180   and PGI affecting C-1 and C-2 (Table 2) (Gilbert *et al.*, 2012). Several findings support this hypothesis.

181   First, among all Δ_i series, Δ_1', $\Delta_{1\text{-}2}$', $\Delta_{1\text{-}3}$', and Δ are not normally distributed (Table S1, negative skew).

182   Second, among these nonnormal series, $\Delta_{1\text{-}2}$', $\Delta_{1\text{-}3}$', and Δ exhibit a change point in 1980 ($\Delta_{1\text{-}2}$': parametric

183   test, $p < 0.001$, nonparametric test, $p < 0.05$; $\Delta_{1\text{-}3}$': parametric test, $p < 0.01$; Δ: parametric test: $p < 0.05$; n

184   = 31). Third, 1983 to 1995 average values of Δ_1', Δ_2', $\Delta_{1\text{-}2}$', and Δ are significantly lower than the average

185   values of 1961 to 1980, while the 1983 to 1995 variance is significantly larger (Table S2). By contrast, Δ_3'

186   does not exhibit significant differences in average value or variance between the two periods. Fourth, Δ_1'

187   and Δ_2' data pertaining to 1983 to 1995 are significantly correlated ($r = 0.67$, $p = 0.01$, $n = 13$). Fifth, ε_{met}

188   approximates average hydrogen isotope fractionation at glucose H^1 and H^2 caused by metabolic processes

189   (Eq. 1). Using simple linear regression modelling, we found significant negative relationships between the

190   1983 to 1995 data of ε_{met} and Δ_1' as well as Δ_2', but not Δ_3' or any other Δ_i (Fig. 3, green circles; Δ_1' ~ ε_{met}:

191    $R^2 = 0.35$, $adjR^2 = 0.29$, $p = 0.03$; Δ_2' ~ ε_{met}: $R^2 = 0.54$, $adjR^2 = 0.50$, $p = 0.004$; Δ_3' ~ ε_{met}: $R^2 = 0.21$, $adjR^2$

192   = 0.13, $p > 0.1$; $n = 13$; Table S3). Our ^{13}C-NMRS data exhibit relatively large measurement errors. Based

193   on estimates of this random error variance, about 88% of the variance in the Δ_1' and Δ_2' data of 1983 to

194   1995 is systematic variance (Table S4). Hence, about 33% and 57% of the systematic variance in Δ_1' and

195   Δ_2' is explained by processes causing ε_{met} variation (0.29/0.88 and 0.5/0.88) while about 67% and 43%,

196   respectively, go back to other processes. Taken together, carbon and hydrogen isotope signals at glucose

197   HC-1 and HC-2 are significantly associated during 1983 to 1995 but not during 1961 to 1980 (Notes S2).

198   The processes introducing these signals cause concerted ^{13}C and deuterium enrichments (Fig. 3A-B).

199

200   *Isotope-environment relationships at tree-ring glucose C-1 to C-3*

201   As evident from our previously published hierarchical cluster analysis and Pearson correlation analyses for

202   the whole period (1961 to 1995), Δ_1', Δ_2', and Δ_3' share common variability (Fig. 1B) (Wieloch *et al.*, 2018).

203   Since Δ_{1-2}' and Δ_{1-3}' exhibit change points in 1980 (see above and Tables S1-2), we analysed the early

204   (1961 to 1980) and late period (1983 to 1995) separately.

205

206   During the late period, Δ_1' and Δ_3' are more closely associated (Fig. 4A; $r = 0.87$, $p = 10^{-4}$, $n = 13$) than Δ_1'

207   and Δ_2' ($r = 0.67$, $p = 0.01$, $n = 13$). While this contrasts with results for the whole period (Fig. 1B), it is

208   consistent with isotope-climate-relationship patterns for the late period. Δ_1' and Δ_3' correlate similarly with

209   numerous climate parameters and periods (Table 3; *VPD*, *PRE*, *SPEI*$_1$ to *SPEI*$_{16}$, *TMP*, *SD*). By contrast,

210   Δ_2' correlates only with one *VPD* period and several *PRE* periods. A model including ε_{met} and growing

211   season *VPD* as cofactors captures most of the systematic variance in Δ_1' of 88% (Table 4, M1; Table S4).

212   Consistent with the findings above (Fig. 3, Table 3), only ε_{met} but not growing season *VPD* contributes

213   significantly to the Δ_2' model whereas only growing season *VPD* but not ε_{met} contributes significantly to the

214   Δ_3' model (Table 4, M2-3). Removing insignificant terms, we find that ε_{met} explains 57% of the systematic

215   variance in Δ_2', while growing season *VPD* explains the entire systematic variance in Δ_3' (Table 4, M4-5;

216   Table S4). The effect of *VPD* on Δ_1' is about twice as large as on Δ_3' (Table 4, M1 versus M5) while the

217   effect of ε_{met} on Δ_1' is about half as large as on Δ_2' (M1 versus M4). Intriguingly, Δ_1' and Δ_3' are affected by

218   processes that respond to growing season *VPD*. *VPD*-dependent processes can account for both the

219   clustering and correlation between Δ_1' and Δ_3' data of 1983 to 1995 (Fig. 4A). By contrast, ε_{met} is significantly

220   correlated only with *PRE* (especially March to July *PRE*) but no other climate parameter (Table S5; Table

221   4, M11). Furthermore, in our Δ_1' and Δ_2' models, ε_{met} can be substituted by March to July *PRE* (Table 4, M1

222   versus M6, M4 versus M7).

223

224   During the early period, Δ_1', Δ_2', and Δ_3' are not significantly correlated (Fig. 4B). Furthermore, isotope-

225   environment models that work for the late period (Table 4, M5-7) do not work for the early period (M8-10).

226   Compared to the late period, we found fewer and weaker isotope-climate correlations (Table 5).

227

228   *Isotope-environment relationships at tree-ring glucose C-4 to C-6*

229   As evident from our previously published hierarchical cluster analysis and Pearson correlation analyses for

230   the whole period, Δ_4', Δ_5', and Δ_6' share common variability, and Δ_5' and Δ_6' are significantly correlated (Fig.

231   1B; $r = 0.61$, $p < 0.001$, $n = 31$) (Wieloch *et al.*, 2018). This significant correlation holds for both the early

232   and late period (Fig. 4). Furthermore, we did not find change points in the Δ_4', Δ_5', and Δ_6' series (see also

233   Tables S1-2). Therefore, we analysed isotope-environment relationships for the whole period. We found

234   that Δ_5' and Δ_6' correlate with numerous climate parameters and periods but most significantly with *RAD*

235   while significant Δ_4'-climate correlations are rare (Table 6). Models including April to September *RAD* and

236   March to October *TMP* as cofactors capture 96% of the systematic variance in Δ_{5-6}', Δ_5', and Δ_6' of 73%,

237   66%, and 45%, respectively (Table 7, M1-3; Δ_{5-6}', $adjR^2 = 0.70$, $p = 10^{-7}$; Δ_5', $adjR^2 = 0.64$, $p = 10^{-6}$; Δ_6',

238    $adjR^2 = 0.43$, $p < 0.001$; $n = 28$; Table S4). Based on *RAD* regression slopes (which are better constrained

239   than *TMP* regression slopes), the ^{13}C discrimination at C-5 is about 1.5 times larger than at C-6 (Table 7,

7

240 M2-3). The model works well for both the early and late period (Table 7, M4-5). Furthermore, consistent

241 with the weak association between Δ_4' and Δ_{5-6}' (Fig. 1B), the model works reasonably well for Δ_4'

242 considering the relatively low systematic variance in Δ_4' of 38% (Table 7, M6; Table S4).

243

244 **Discussion**

245 *Intramolecular carbon isotope analysis of tree-ring glucose yields information about metabolic variability*

246 *and water status of both leaves and stems*

247 We found evidence for processes affecting Δ_1' and Δ_3' which respond to *VPD* (Table 4, M1, M3, M5).

248 Intriguingly, we also found evidence for processes simultaneously affecting ε_{met}, Δ_1', and Δ_2' which respond

249 to *PRE* but not *VPD* (Table S5; Table 4, M1, M2, M4, M6, M7, M11). This sensitivity to different hydrological

250 properties may be explained by the fact that stem capacitance can buffer stem water status against changes

251 in *VPD* (McCulloh *et al.*, 2019), whereas leaf water status is tightly coupled to *VPD* (Grossiord *et al.*, 2020).

252 Changes in *PRE* will affect soil water potential and hence both stem and leaf water status. Variability in leaf

253 water status may be impacted more by *VPD* than by soil water status which would explain why *VPD* is the

254 best predictor of the intercorrelated processes affecting Δ_1' and Δ_3'. By contrast, *VPD*-insensitive processes

255 affecting ε_{met}, Δ_1', and Δ_2' may reside in stems. Hence, we propose intramolecular carbon and hydrogen

256 isotope analysis of tree-ring glucose yields information about metabolic variability and water status not only

257 of leaves but also of stems. *PRE*-dependent systemic changes in enzyme expression can be considered

258 as an alternative explanation.

259

260 *Isotope fractionation mechanisms in leaves affecting tree-ring glucose C-1 to C-3*

261 The Δ_{1-2}' and Δ_{1-3}' series exhibit change points in 1980, i.e., their frequency distributions do not align with

262 the properties of a single theoretical probability distribution ('Results'; Tables S1-2). Consequently, we

263 investigated the early (1961 to 1980) and late period (1983 to 1995) separately. During the late period, Δ_1'

264 and Δ_3' are significantly intercorrelated (Fig. 4A) and correlate negatively with *VPD* and positively with short-

265 term *SPEI* whereas Δ_2' lacks most of these correlations (Table 3). Furthermore, during the late period,

266 growing season *VPD* accounts for a significant fraction of the systematic variance in Δ_1' and the entire

267 systematic variance in Δ_3' but does not contribute significantly to explaining Δ_2' (Table 4, M1, M2, M5; Table

268 S4). Hence, increasing *VPD* during 1983 to 1995 causes ^{13}C enrichments at tree-ring glucose C-1 and C-

269 3 but not C-2. At C-1, the effect is about twice as large as at C-3 (Table 4, M1 and M5).

270

271 As discussed above, the *VPD*-dependent processes affecting Δ_1' and Δ_3' are likely located in leaves.

272 Qualitatively, *VPD*-induced ^{13}C enrichments at C-1 and C-3 are consistent with the mechanisms of diffusion-

273 rubisco fractionation (see 'Introduction'). However, diffusion-rubisco fractionation affects all glucose carbon

274 positions equally (Wieloch *et al.*, 2018). Hence, the unequal *VPD* response of Δ_1', Δ_2', and Δ_3' points to

275 post-rubisco fractionations. In the following, we assume Δ_3' variation derives entirely from diffusion-rubisco

276 fractionation and argue *VPD*-dependent isotope fractionation at PGI and G6PD in leaf chloroplasts and the

8

277   cytosol may exert additional control over $Δ_1$' and $Δ_2$' variability. Generally, variability in PGI fractionation

278   depends on three biochemical properties: (i) the equilibrium status of the PGI reaction, and relative flux of

279   the PGI reactants (ii) F6P and (iii) G6P into competing metabolic pathways (Figs. 2 and 5):

280

281   (i) PGI reversibly converts F6P into G6P (Fig. 5A). Under nonstress conditions, the PGI reaction in

282   chloroplasts is strongly displaced from equilibrium on the side of F6P (Dietz, 1985; Gerhardt *et al.*, 1987;

283   Kruckeberg *et al.*, 1989; Schleucher *et al.*, 1999; Wieloch *et al.*, 2022a; Wieloch, 2022). With decreasing p_i,

284   however, the reaction moves towards equilibrium (Dietz, 1985; Wieloch *et al.*, 2022a). This shift is

285   accompanied by ^{13}C increases at C-1 and C-2 of G6P (Table 2) which will be transmitted to downstream

286   derivatives such as starch and tree-ring glucose (Wieloch *et al.*, 2018). In isohydric species such as *Pinus*

287   *nigra*, p_i decreases with drought due to stomatal closure (McDowell *et al.*, 2008). Here, we found stronger

288   *VPD*-induced ^{13}C increases at tree-ring glucose C-1 than at C-3. This is consistent with the PGI-related

289   isotope shift expected at C-1. However, the apparent absence of the diffusion-rubisco signal from C-2

290   contrasts with the expected isotope shift. That said, in *Phaseolus vulgaris*, the ratio of leaf sucrose-to-starch

291   carbon partitioning was shown to increase steeply with decreasing p_i (Sharkey *et al.*, 1985). Hence, the

292   relative contribution of chloroplastic G6P and its isotope composition to downstream metabolism may

293   decrease with increasing *VPD* reducing the influence of the mechanism described on $Δ_1$' and $Δ_2$' variation.

294

295   (ii) In natural systems, leaf nighttime respiration is increased under drought (Fig. 5B; Schmiege *et al.*, 2023).

296   Furthermore, in the dark, the cytosolic PGI reaction was found to be near equilibrium (Gerhardt *et al.*, 1987).

297   Consequently, F6P would be ^{13}C depleted at C-1 but ^{13}C enriched at C-2 relative to the corresponding G6P

298   positions (Table 2). Increasing relative F6P flux into mitochondrial respiration would then result in ^{13}C

299   increases at C-1 and ^{13}C decreases at C-2 of G6P and downstream derivatives. Thus, this mechanism is

300   consistent with both observations, stronger *VPD*-induced ^{13}C increases at tree-ring glucose C-1 compared

301   to C-3 and the apparent absence of the diffusion-rubisco signal from C-2.

302

303   (iii) While carbon assimilation commonly decreases with drought (McDowell *et al.*, 2008), the activity of leaf-

304   cytosolic G6PD increases (Fig. 5C; Landi *et al.*, 2016). This can be expected to result in increasing relative

305   G6P flux into the OPPP. While some authors reported that the cytosolic PGI reaction in illuminated leaves

306   is in equilibrium (Gerhardt *et al.*, 1987) others found displacements from equilibrium (Leidreiter *et al.*, 1995;

307   Schleucher *et al.*, 1999; Szecowka *et al.*, 2013). Hence, PGI-related isotope shifts in tree-ring glucose

308   resulting from G6P flux into the leaf-cytosolic OPPP are hard to predict (Table 2). By contrast, the

309   unidirectional conversion of G6P to 6-phosphogluconolactone catalysed by G6PD proceeds faster with ^{12}C-

310   1 than ^{13}C-1 G6P ($k_{^{12}C}/k_{^{13}C} = 1.0165$) (Hermes *et al.*, 1982). Hence, increasing relative flux through the

311   leaf-cytosolic OPPP may contribute to the stronger *VPD*-induced ^{13}C increases at tree-ring glucose C-1

312   compared to C-3.

313

9

314 Aside from these mechanisms, there are others that might introduce Δ_1' and Δ_2' variation. For instance, we
315 recently reported evidence consistent with increasing relative flux through the chloroplastic OPPP in
316 response to decreasing p_i under illumination (Fig. 5A; Wieloch *et al.*, 2022a, 2023). Furthermore, under
317 illumination, chloroplastic F6P is used for both RuBP regeneration and starch biosynthesis (Fig. 5A).
318 Increasing *VPD* promotes photorespiration resulting in increasing RuBP regeneration relative to carbon
319 export from the Calvin-Benson cycle into sinks such as starch.

320

321 The mechanisms described above should also introduce hydrogen isotope signals because of the hydrogen
322 isotope effects of G6PD affecting G6P H[1] (Hermes *et al.*, 1982) and PGI affecting G6P H[2] (Table 2, Fig. 5).
323 However, growing season *VPD* neither correlates with ε_{met} pertaining to tree-ring glucose H[1] nor H[2] (Tables
324 S5-6). Hence, either G6PD and PGI are not the sources of *VPD*-dependent carbon isotope fractionation in
325 Δ_1' (and Δ_2') or the corresponding hydrogen isotope signals were washed out after introduction. Washout
326 at H[1] may occur during equilibration of F6P with mannose 6-phosphate by phosphomannose isomerase
327 (*cf.* Topper, 1957). Similarly, complete washout at H[2] may occur when the leaf-cytosolic PGI reaction is in
328 equilibrium (Notes S3). Previously, this latter process was invoked (among others) to explain why a whole-
329 molecule deuterium depletion observed in leaf starch was not transmitted to nocturnal sucrose
330 ('Introduction'; Wacker, 2022). As each conversion by PGI was found to be associated with a 0 to 50%
331 probability for hydrogen exchange with the medium (Noltmann, 1972), partial washout of existing hydrogen
332 isotope signals may also occur under non-equilibrium conditions (Notes S3).

333

334 In the mechanisms described above, we assumed diffusion-rubisco fractionation contributes to *VPD*-
335 dependent Δ_i' variation. However, diffusion-rubisco fractionation affects all glucose carbon positions equally
336 (Wieloch *et al.*, 2018). Since merely two out of six glucose carbon positions carry *VPD*-dependent isotope
337 variation, the question arises of whether the diffusion-rubisco signal was already below the detection level
338 on introduction. If this were the case, then *VPD*-dependent Δ_1' and Δ_3' variation would originate entirely
339 from post-rubisco processes. Furthermore, post-rubisco processes that were previously invoked to explain
340 the absence of the diffusion-rubisco signal from C-4, C-5, and C-6 (see 'Introduction') would not occur.

341

342 *Isotope fractionation mechanisms in stems affecting tree-ring glucose HC-1 and HC-2*

343 Previously, we found a change point in ε_{met} in 1980 (Wieloch *et al.*, 2022b). Here, we found the same
344 change point in Δ_{1-2}' ('Results'). Consistent with this, Δ_1' and Δ_2' data of 1983 to 1995 exhibit a significantly
345 lower average value and a significantly larger variance than those of 1961 to 1980 (Tables S1-2).
346 Furthermore, Δ_1' and Δ_2' are significantly correlated during the late (Fig. 4B) but not the early period (Fig.
347 4A), and ε_{met} accounts for a significant fraction of the variance of both Δ_1' and Δ_2' during the late period
348 (Table 4, M1, M4; Figs. 3A-B). In Δ_2', the ε_{met} effect is about twice as large as in Δ_1'. Processes affecting
349 ε_{met}, Δ_1', and Δ_2' simultaneously respond to *PRE* but not *VPD* (Table S5; Table 4, M1, M2, M4, M6, M7,
350 M11). Δ_1' and Δ_2' respond to March to July *PRE* during the late but not the early period (Table 4, M9-10).

351 Previously, we reported evidence suggesting the groundwater table before 1980 was high enough to
352 prevent metabolic changes causing ε_{met} variation (Wieloch *et al.*, 2022b). By extension, this should also
353 explain the properties of Δ_1' and Δ_2' listed above. That is, since the trees had access to groundwater during
354 the early period, metabolic shifts that can cause intercorrelated variation in ε_{met}, Δ_1', and Δ_2' were not
355 induced.

356

357 Processes causing intercorrelated variation in ε_{met}, Δ_1', and Δ_2' are probably located in the stem (see the
358 first section of the 'Discussion'). The ε_{met} signal is present at glucose H^1 and, considerably more strongly,
359 at H^2 (range: 64‰ and 240‰, respectively; 1983 to 1995). In the biochemical pathway leading to tree-ring
360 cellulose, PGI is the last enzyme acting on precursors of glucose H^2 (Figs. 2 and 5D). With each conversion
361 by PGI, there is a probability for hydrogen exchange with the medium of 0 to 50% (Noltmann, 1972). Thus,
362 if we assume *Pinus nigra* stem PGI exchanges hydrogen with the medium as does spinach leaf PGI
363 (Fedtke, 1969) and the reaction is in equilibrium, then any deuterium signal at G6P H^2 will be washed out.
364 Among all H-C positions of tree-ring glucose, the deuterium abundance at H^2 is neither exceptionally high
365 nor low during 1961 to 1980 whereas it is exceptionally high (and exceptionally variable) during 1983 to
366 1995 (Fig. 6). This indicates that the PGI reaction was close to or in equilibrium during 1961 to 1980 but
367 displaced from equilibrium on the side of G6P during 1983 to 1995 (Table 2). Additionally, shifts of the PGI
368 reaction away from equilibrium towards the side of G6P should cause ^{13}C enrichment at G6P C-1 and C-2
369 (Δ_1' and Δ_2' decreases), and Δ_2' should decrease 3 times more than Δ_1' (Table 2). Consistent with this, we
370 found negative relationships between ε_{met} and Δ_1', as well as Δ_2' (Table 4, M1 and M4). However, Δ_2'
371 decreases only 1.88 times more than Δ_1', but this best estimate is associated with a relatively large error
372 (SE interval: 1.04 to 3.45). That said, the offset from 3 is likely explained by increasing relative flux through
373 the OPPP accompanying the putative PGI reaction shift (Figs. 2 and 5D). This is because G6P to 6-
374 phosphogluconolactone conversion by G6PD exhibit ^{13}C and D isotope effects ($k_{^{12}C}/k_{^{13}C} =$
375 $1.0165, k_H/k_D = 2.97$) (Hermes *et al.*, 1982). Hence, increasing relative OPPP flux causes ^{13}C enrichment
376 at G6P C-1 (Δ_1' decreases) and deuterium enrichment at G6P H^1. This is consistent with both the apparently
377 decreased PGI effects ratio (1.88 instead of 3) and, more importantly, ε_{met} increases at glucose H^1 of up to
378 64‰ during 1983 to 1995 (Fig. 6).

379

380 Sucrose translocated from leaves can be split into UDP-glucose and fructose via sucrose synthase or
381 glucose and fructose via invertase (Fig. 2). UDP-glucose entering tree-ring cellulose biosynthesis directly
382 via sucrose synthase is protected from isotope fractionation by PGI and G6PD. However, in stems of
383 juvenile *Quercus petraea* and *Picea abies*, at least 79% and 43% of the precursors of tree-ring glucose
384 went through PGI catalysis, respectively (Augusti *et al.*, 2006). Theoretically, shifts of the PGI reaction away
385 from equilibrium towards the side of G6P can cause ε_{met} increases at glucose H^2 of up to 611‰ (Notes S3,
386 hydrogen exchange with the medium not considered). With 43% and 79% of all precursors of tree-ring
387 glucose undergoing PGI catalysis, ε_{met} increases at glucose H^2 of up to 263‰ and 483‰ are possible,

11

388   respectively. Thus, the PGI-related fractionation mechanism proposed here can potentially cause

389   previously reported ε_{met} increases at glucose H^2 of up to 240‰ (Wieloch *et al.*, 2022b). Shifts in sucrose

390   cleavage by sucrose synthase versus invertase may exert additional control on the ε_{met} signal at glucose

391   H^2.

392

393   Based on results and interpretations presented above, decreasing stem water content is associated with

394   both increasing OPPP flux and a shift of the PGI reaction away from equilibrium towards the side of G6P

395   corresponding to low relative F6P concentration (Fig. 5D). We propose these concerted shifts may ensure

396   redox homeostasis and balanced substrate supply to glycolysis as follows. In heterotrophic tissue, NADPH

397   from the OPPP is believed to be central for maintaining redox homeostasis (Fig. 2) (Stincone *et al.*, 2015).

398   Flux through the OPPP is regulated at G6PD. Heterotrophic G6PD activity reportedly increases with drought

399   (Liu *et al.*, 2013; Wang *et al.*, 2016, 2020), oxidative load (Wang *et al.*, 2016, 2020; Li *et al.*, 2020), NADPH

400   demand (Wendt *et al.*, 2000; Esposito *et al.*, 2001; Castiglia *et al.*, 2015), and abscisic acid concentration

401   (Cardi *et al.*, 2011; Wang *et al.*, 2016). Decreasing stem water content may cause increasing OPPP flux

402   via increasing abscisic acid concentration (Brunetti *et al.*, 2020), and possibly increasing oxidative load

403   increasing the demand for NADPH. In turn, increasing OPPP flux results in increasing supply of pentose

404   phosphates which may feed into glycolysis via the reductive part of the pentose phosphate pathway (Figs.

405   2 and 5D). This would reduce the demand for glycolytic substrates supplied via PGI. The shift of the PGI

406   reaction away from equilibrium towards the side of G6P may reflect this decreased demand and result from

407   PGI downregulation by intermediates of the pentose phosphate pathway such as erythrose 4-phosphate,

408   ribulose 5-phosphate, and 6-phosphogluconate (Parr, 1956; Grazi *et al.*, 1960; Salas *et al.*, 1965).

409   Furthermore, relative changes in G6P-to-F6P supply versus consumption may contribute to the shift of the

410   PGI reaction. For instance, while starch storage consumes G6P, remobilisation supplies G6P (Noronha *et*

411   *al.*, 2018). Under drought, the storage-to-remobilisation balance may tilt towards remobilisation (Mitchell *et*

412   *al.*, 2013; Thalmann & Santelia, 2017; Tsamir-Rimon *et al.*, 2021). Consequently, the PGI reaction may

413   move towards the side of G6P. Similarly, we previously reported below-average tree-ring widths for years

414   in which the PGI reaction is on the side of G6P (Wieloch *et al.*, 2022b). Hence, in these years, G6P

415   consumption by growth may have been reduced while F6P consumption by downstream metabolism may

416   have been maintained.

417

418   *1961 to 1980: A period of homeostasis with respect to processes affecting Δ_1', Δ_2', Δ_3', and ε_{met}*

419   During 1961 to 1980, Δ_1', Δ_2', and Δ_3' are not significantly correlated which contrasts with the period 1983

420   to 1995 (Figs. 4a-b). Similarly, relationships of Δ_1' and Δ_3' with *VPD* and Δ_1' and Δ_2' with *PRE* observed

421   during the late period are largely absent during the early period (Tables 3-5) even though there is no

422   difference in the magnitude of *VPD* and *PRE* variability between these periods (Fig. S1). Like $\Delta_{1\text{-}2}'$ and $\Delta_{1\text{-}}$

423    $_3'$, ε_{met} exhibits a change point in 1980 and responds to *PRE* after but not before 1980 (Wieloch *et al.*,

424   2022b). This shift in ε_{met} sensitivity was attributed to long-term drought which intensified over the study

425 period and proposedly lead to a groundwater depletion below a critical level in 1980 (Wieloch *et al.*, 2022b).

426 By extension, this groundwater depletion might also explain the insensitivity of Δ_1' and Δ_3' to *VPD* and Δ_1'

427 and Δ_2' to *PRE* during 1961 to 1980 and their sensitivity from 1983 onwards. Thus, while the trees had

428 access to groundwater, leaf- and stem-level processes affecting Δ_1', Δ_2', Δ_3' and ε_{met} could apparently

429 maintain homeostasis despite changing atmospheric conditions.

430

431 *Isotope fractionation mechanisms in leaves affecting tree-ring glucose C-5 and C-6*

432 No change points were detected in Δ_5' and Δ_6' ('Results'; Tables S1-2). Furthermore, Δ_5' and Δ_6' remain

433 significantly correlated across the entire study period (Figs. 1B and 4A-B), and *RAD* is the most influential

434 environmental cofactor (Table 6). Models including *RAD* and *TMP* as cofactors capture most of the

435 systematic variance in $\Delta_{5\text{-}6}$', Δ_5', and Δ_6' (Table 7, M1-3; Table S4). These relationships hold for both the

436 early and late study period (Table 7, M4-5) with Δ_5' effects being about 1.5-fold larger than Δ_6' effects (M2

437 versus M3, SE interval: 1.1 to 2.28).

438

439 Previously, we reported a negative relationship between tree-ring glucose $\Delta_{5\text{-}6}$' and reconstructed

440 tropospheric O_3 concentration ('Introduction', Wieloch *et al.*, 2022c). Light stimulates tropospheric O_3

441 formation (Lu *et al.*, 2019). This may explain the negative relationship between tree-ring glucose $\Delta_{5\text{-}6}$' and

442 *RAD* reported here (Table 7, M1-3). Furthermore, we previously explained the absence of the diffusion-

443 rubisco signal from glucose C-5 and C-6 (*inter alia*) by interaction between photorespiration and the TCAC

444 ('Introduction', Wieloch *et al.*, 2022c). As *TMP* increases, photorespiration increases more than

445 photosynthesis (Long, 1991). This may result in decreasing flux of PEP into the TCAC ('Introduction') and

446 explain the positive relationship between tree-ring glucose $\Delta_{5\text{-}6}$' and *TMP* reported here (Table 7, M1-3).

447

448 *Isotope fractionation mechanisms in leaves affecting tree-ring glucose C-4*

449 As for Δ_5' and Δ_6', no change point was detected in Δ_4' ('Results'; Tables S1-2). Considering the entire

450 study period, Δ_4' is weakly associated with $\Delta_{5\text{-}6}$' (Fig. 1B). Consistent with this, the $\Delta_{5\text{-}6}$'-climate model works

451 reasonably well for Δ_4' considering the relatively low systematic variance in Δ_4' of 38% (Table 7, M1 and

452 M6; Table S4). Introduction of the Δ_4' and $\Delta_{5\text{-}6}$' signals proposedly involves leaf-level consumption of PGA

453 and PEP by downstream metabolism, respectively (Wieloch *et al.*, 2021, 2022c). Since PGA is a precursor

454 of PEP (Fig. 2), our previously proposed theories of signal introduction are in line with the observation that

455 Δ_4', Δ_5' and Δ_6' are associated and respond to the same environmental parameters.

456

457 **Conclusions and future directions**

458 Dual-isotope-environment analysis was used to deconvolute isotope signals and provide several new

459 insights into plant isotope fractionation. First, the diffusion-rubisco signal was previously shown to be absent

460 from tree-ring glucose C-4 to C-6 (Wieloch *et al.*, 2021, 2022c) but believed to be present at C-1 to C-3

461 (Wieloch *et al.*, 2018). Here, this signal was found to also be absent from C-2. Second, isotope fractionation

13

462   beyond leaves is commonly considered to be constant for any given species (Roden *et al.*, 2000; Gagen *et*

463   *al.*, 2022). However, our results suggest a significant part of the carbon and hydrogen isotope variation in

464   tree-ring glucose originates in stems from processes affecting Δ_1', Δ_2', and ε_{met} simultaneously. Third, *VPD*

465   affects Δ_1' and Δ_3' and *PRE* affects Δ_1', Δ_2', and ε_{met} (Table 4). These relationships proposedly reflect water

466   content variability in leaves and stems, respectively. They apply to the late but not the early study period

467   consistent with the finding of a change point in both the ε_{met} (Wieloch *et al.*, 2022b) and Δ_{1-3}' series (see

468   above). This change point proposedly marks the crossing of a physiologically relevant groundwater

469   threshold (Wieloch *et al.*, 2022b). Additionally, we reported Δ_{5-6}' relationships with *RAD* and *TMP* which

470   apply to the entire study period (Table 4). These latter relationships are consistent with previously proposed

471   isotope fractionation mechanisms (Wieloch *et al.*, 2022c). By contrast, we here revised and expanded our

472   previous theory on the mechanisms introducing Δ_1', Δ_2', Δ_3', and ε_{met} variability. Given the multitude of

473   isotope-environment relationships (including change-point responses), intramolecular carbon isotope

474   analysis has a remarkable potential for reconstructions of environmental conditions (*VPD*, *PRE*, *RAD*, *TMP*,

475   soil moisture, groundwater thresholds, tropospheric O_3 concentration), tissue water content (leaf, stem),

476   metabolic flux variability (various processes), and ecophysiological properties such as intrinsic water-use

477   efficiency across space and time. Complementing hydrogen isotope analysis is expected to significantly

478   enhance these capabilities.

479

480   Understanding isotope fractionation mechanisms is central for retrospective studies of plant physiology and

481   climate based on tree-ring isotope data, and there is considerable room for improvement as shown above.

482   Research in several largely unexploited areas is needed to make progress. First, there is a basic need for

483   more *in vitro* data on intramolecular isotope effects of enzyme reactions including the reactions catalysed

484   by triosephosphate isomerase, transketolase, PEPC, PK, and DAHPS. Second, intramolecular isotope

485   analyses of leaf metabolites including starch and sucrose from both controlled and natural environments

486   are needed to generate a baseline for mechanistic studies of isotope fractionation along the pathway from

487   leaves to wood. Additionally, intramolecular isotope analysis of metabolites from wood slices acclimated to

488   different ambient conditions (e.g., wet versus dry, varying sucrose supply) will be insightful. Third, combined

489   analysis of intramolecular ^{13}C and deuterium data can help to separate isotope signals. Fourth, genetic

490   modification of key enzymes may help to test proposed isotope fractionation mechanisms *in vivo*. Fifth,

491   intramolecular isotope fractionation affecting tree-ring glucose is complex (see above). Software programs

492   such as QIRN enable the convenient simulation of natural isotope abundances in complex metabolic

493   networks (Mueller *et al.*, 2022). If expanded, these programs may help to extract metabolic information from

494   intramolecular tree-ring isotope data. This would require routines enabling control of relative flux at

495   metabolic branchpoints by optimising regressions between (i) relative branchpoint flux and environmental

496   parameters and (ii) simulated and observed isotope data. In summary, intramolecular isotope analysis has

497   an enormous potential to advance our knowledge about isotope fractionation mechanisms, plant

498   ecophysiology, and paleoclimatology.

504   **Author Contributions**

505   Conceptualisation: TW; Investigation: TW with input from all authors; Visualization: TW; Development of

506   isotope theory: TW; Project administration: TW; Writing: TW with input from all authors.

507

508   **Competing interests**

509   None declared.

510

511   **Data availability**

512   The authors declare that the data supporting the findings of this study are available within the paper and its

513   supplementary information files.

514

515   **References**

516   **Abtew W, Melesse AM**. **2013**. Chapter 5 - Vapor pressure calculation methods. In: Evaporation and
517   Evapotranspiration. Springer Verlag, 53–62.

518   **Augusti A, Betson TR, Schleucher J**. **2006**. Hydrogen exchange during cellulose synthesis distinguishes
519   climatic and biochemical isotope fractionations in tree rings. *New Phytologist* **172**: 490–499.

520   **Badeck FW, Tcherkez G, Nogues S, Piel C, Ghashghaie J**. **2005**. Post-photosynthetic fractionation of
521   stable carbon isotopes between plant organs-a widespread phenomenon. *Rapid Communications in Mass*
522   *Spectrometry* **19**: 1381–1391.

523   **Beguería S, Vicente-Serrano SM, Angulo-Martínez M**. **2010**. A multiscalar global drought dataset: The
524   SPEIbase. *Bulletin of the American Meteorological Society* **91**: 1351–1356.

525   **Betz GA, Gerstner E, Stich S, Winkler B, Welzl G, Kremmer E, Langebartels C, Heller W, Sandermann**
526   **H, Ernst D**. **2009**. Ozone affects shikimate pathway genes and secondary metabolites in saplings of
527   European beech (*Fagus sylvatica* L.) grown under greenhouse conditions. *Trees* **23**: 539–553.

528   **Brunetti C, Savi T, Nardini A, Loreto F, Gori A, Centritto M**. **2020**. Changes in abscisic acid content
529   during and after drought are related to carbohydrate mobilization and hydraulic recovery in poplar stems.
530   *Tree Physiology* **40**: 1043–1057.

531   **Cardi M, Chibani K, Cafasso D, Rouhier N, Jacquot J-P, Esposito S**. **2011**. Abscisic acid effects on
532   activity and expression of barley (*Hordeum vulgare*) plastidial glucose-6-phosphate dehydrogenase.
533   *Journal of Experimental Botany* **62**: 4013–4023.

534 **Castiglia D, Cardi M, Landi S, Cafasso D, Esposito S**. **2015**. Expression and characterization of a
535 cytosolic glucose 6 phosphate dehydrogenase isoform from barley (*Hordeum vulgare*) roots. *Protein*
536 *Expression and Purification* **112**: 8–14.

537 **Cernusak LA, Tcherkez G, Keitel C, Cornwell WK, Santiago LS, Knohl A, Barbour MM, Williams DG,**
538 **Reich PB, Ellsworth DS, *et al.* 2009**. Why are non-photosynthetic tissues generally ^{13}C enriched compared
539 with leaves in C_3 plants? Review and synthesis of current hypotheses. *Functional Plant Biology* **36**: 199–
540 213.

541 **Cossar JD, Rowell P, Stewart WDP**. **1984**. Thioredoxin as a modulator of glucose-6-phosphate
542 dehydrogenase in a N_2-fixing cyanobacterium. *Microbiology* **130**: 991–998.

543 **Craig H**. **1953**. The geochemistry of the stable carbon isotopes. *Geochimica Et Cosmochimica Acta* **3**: 53–
544 92.

545 **Dietz K-J**. **1985**. A possible rate-limiting function of chloroplast hexosemonophosphate isomerase in starch
546 synthesis of leaves. *Biochimica et Biophysica Acta* **839**: 240–248.

547 **Dizengremel P**. **2001**. Effects of ozone on the carbon metabolism of forest trees. *Plant Physiology and*
548 *Biochemistry* **39**: 729–742.

549 **Esposito S, Carfagna S, Massaro G, Vona V, Di Martino Rigano V**. **2001**. Glucose-6-phosphate
550 dehydrogenase in barley roots: kinetic properties and localisation of the isoforms. *Planta* **212**: 627–634.

551 **Evans JR, Farquhar GD, Sharkey TD, Berry JA**. **1986**. Carbon isotope discrimination measured
552 concurrently with gas exchange to investigate CO_2 diffusion in leaves of higher plants. *Australian Journal*
553 *of Plant Physiology* **13**: 281–292.

554 **Fan Y, van den Dool H**. **2004**. Climate Prediction Center global monthly soil moisture data set at 0.5°
555 resolution for 1948 to present. *Journal of Geophysical Research: Atmospheres* **109**.

556 **Farquhar GD**. **1983**. On the nature of carbon isotope discrimination in C_4 species. *Australian Journal of*
557 *Plant Physiology* **10**: 205–226.

558 **Farquhar GD, O'Leary MH, Berry JA**. **1982**. On the relationship between carbon isotope discrimination
559 and the intercellular carbon dioxide concentration in leaves. *Australian Journal of Plant Physiology* **9**: 121–
560 137.

561 **Farquhar GD, Richards RA**. **1984**. Isotopic composition of plant carbon correlates with water-use
562 efficiency of wheat genotypes. *Australian Journal of Plant Physiology* **11**: 539–552.

563 **Fedtke C**. **1969**. Intramolecular hydrogen transfer in isomerisation reactions of sugar phosphates in the
564 Calvin cycle. In: Metzner H, ed. Progress in Photosynthesis Research. Tübingen, 1597–1603.

565 **Gagen M, Battipaglia G, Daux V, Duffy J, Dorado-Liñán I, Hayles LA, Martínez-Sancho E, McCarroll**
566 **D, Shestakova TA, Treydte K**. **2022**. Climate signals in stable isotope tree-ring records. In: Siegwolf RTW,
567 Brooks JR, Roden J, Saurer M, eds. Stable isotopes in tree tings: Inferring physiological, climatic and
568 environmental responses. Cham: Springer International Publishing, 537–579.

16

Gerhardt R, Stitt M, Heldt HW. **1987**. Subcellular metabolite levels in spinach leaves: Regulation of sucrose synthesis during diurnal alterations in photosynthetic partitioning. *Plant Physiology* **83**: 399–407.

Gilbert A, Robins RJ, Remaud GS, Tcherkez G. **2012**. Intramolecular ^{13}C pattern in hexoses from autotrophic and heterotrophic C_3 plant tissues. *Proceedings of the National Academy of Sciences of the United States of America* **109**: 18204–18209.

Grazi E, De Flora A, Pontremoli S. **1960**. The inhibition of phosphoglucose isomerase by D-erythrose 4-phosphate. *Biochemical and Biophysical Research Communications* **2**: 121–125.

Grossiord C, Buckley TN, Cernusak LA, Novick KA, Poulter B, Siegwolf RTW, Sperry JS, McDowell NG. **2020**. Plant responses to rising vapor pressure deficit. *New Phytologist* **226**: 1550–1566.

Hermes JD, Roeske CA, O'Leary MH, Cleland WW. **1982**. Use of multiple isotope effects to determine enzyme mechanisms and intrinsic isotope effects. Malic enzyme and glucose 6-phosphate dehydrogenase. *Biochemistry* **21**: 5106–5114.

Hobbie EA, Werner RA. **2004**. Intramolecular, compound-specific, and bulk carbon isotope patterns in C_3 and C_4 plants: a review and synthesis. *New Phytologist* **161**: 371–385.

Janzik I, Preiskowski S, Kneifel H. **2005**. Ozone has dramatic effects on the regulation of the prechorismate pathway in tobacco (*Nicotiana tabacum* L. cv. Bel W3). *Planta* **223**: 20–27.

Klein Tank AMG, Wijngaard JB, Können GP, Böhm R, Demarée G, Gocheva A, Mileta M, Pashiardis S, Hejkrlik L, Kern-Hansen C, *et al.* 2002. Daily dataset of 20th-century surface air temperature and precipitation series for the European Climate Assessment. *International Journal of Climatology* **22**: 1441–1453.

Kruckeberg AL, Neuhaus HE, Feil R, Gottlieb LD, Stitt M. **1989**. Decreased-activity mutants of phosphoglucose isomerase in the cytosol and chloroplast of *Clarkia xantiana*. *The Biochemical Journal* **261**: 457–467.

Landi S, Nurcato R, De Lillo A, Lentini M, Grillo S, Esposito S. **2016**. Glucose-6-phosphate dehydrogenase plays a central role in the response of tomato (*Solanum lycopersicum*) plants to short and long-term drought. *Plant Physiology and Biochemistry* **105**: 79–89.

Leavitt SW, Roden J. **2022**. Isotope dendrochronology: Historical perspective. In: Siegwolf RTW, Brooks JR, Roden J, Saurer M, eds. Stable isotopes in tree rings: Inferring physiological, climatic and environmental Responses. Cham: Springer International Publishing, 3–20.

Leidreiter K, Kruse A, Heineke D, Robinson DG, Heldt H-W. **1995**. Subcellular volumes and metabolite concentrations in potato (*Solanum tuberosum* cv. Désirée) leaves. *Botanica Acta* **108**: 439–444.

Li C, Wei M, Ge Y, Zhao J, Chen Y, Hou J, Cheng Y, Chen J, Li J. **2020**. The role of glucose-6-phosphate dehydrogenase in reactive oxygen species metabolism in apple exocarp induced by acibenzolar-S-methyl. *Food Chemistry* **308**: 125663.

Liu J, Wang X, Hu Y, Hu W, Bi Y. **2013**. Glucose-6-phosphate dehydrogenase plays a pivotal role in tolerance to drought stress in soybean roots. *Plant Cell Reports* **32**: 415–29.

605 **Long SP**. **1991**. Modification of the response of photosynthetic productivity to rising temperature by
606 atmospheric CO_2 concentrations: Has its importance been underestimated? *Plant, Cell & Environment* **14**:
607 729–739.

608 **Lu X, Zhang L, Shen L**. **2019**. Meteorology and climate influences on tropospheric ozone: a review of
609 natural sources, chemistry, and transport patterns. *Current Pollution Reports* **5**: 238–260.

610 **McCulloh KA, Domec J-C, Johnson DM, Smith DD, Meinzer FC**. **2019**. A dynamic yet vulnerable
611 pipeline: Integration and coordination of hydraulic traits across whole plants. *Plant, Cell & Environment* **42**:
612 2789–2807.

613 **McDowell N, Pockman WT, Allen CD, Breshears DD, Cobb N, Kolb T, Plaut J, Sperry J, West A,**
614 **Williams DG,** *et al.* **2008**. Mechanisms of plant survival and mortality during drought: why do some plants
615 survive while others succumb to drought? *New Phytologist* **178**: 719–739.

616 **Mitchell PJ, O'Grady AP, Tissue DT, White DA, Ottenschlaeger ML, Pinkard EA**. **2013**. Drought
617 response strategies define the relative contributions of hydraulic dysfunction and carbohydrate depletion
618 during tree mortality. *New Phytologist* **197**: 862–872.

619 **Mueller EP, Wu F, Sessions AL**. **2022**. Quantifying Isotopologue Reaction Networks (QIRN): A modelling
620 tool for predicting stable isotope fractionations in complex networks. *Chemical Geology* **610**: 121098.

621 **Noltmann EA**. **1972**. 9 Aldose-ketose isomerases. In: Boyer PD, ed. The Enzymes. Academic Press, 271–
622 354.

623 **Noronha H, Silva A, Dai Z, Gallusci P, Rombolà AD, Delrot S, Gerós H**. **2018**. A molecular perspective
624 on starch metabolism in woody tissues. *Planta* **248**: 559–568.

625 **Parr CW**. **1956**. Inhibition of phosphoglucose isomerase. *Nature* **178**: 1401.

626 **Preiser AL, Fisher N, Banerjee A, Sharkey TD**. **2019**. Plastidic glucose-6-phosphate dehydrogenases
627 are regulated to maintain activity in the light. *Biochemical Journal* **476**: 1539–1551.

628 **Roden JS, Lin G, Ehleringer JR**. **2000**. A mechanistic model for interpretation of hydrogen and oxygen
629 isotope ratios in tree-ring cellulose. *Geochimica et Cosmochimica Acta* **64**: 21–35.

630 **Roeske CA, O'Leary MH**. **1984**. Carbon isotope effects on the enzyme-catalyzed carboxylation of ribulose
631 bisphosphate. *Biochemistry* **23**: 6275–6284.

632 **Rose IA, O'Connell EL**. **1961**. Intramolecular hydrogen transfer in the phosphoglucose isomerase
633 reaction. *The Journal of Biological Chemistry* **236**: 3086–3092.

634 **Salas M, Vinuela E, Sols A**. **1965**. Spontaneous and enzymatically catalyzed anomerization of glucose 6-
635 phosphate and anomeric specificity of related enzymes. *Journal of Biological Chemistry* **240**: 561–568.

636 **Schleucher J, Vanderveer P, Markley JL, Sharkey TD**. **1999**. Intramolecular deuterium distributions
637 reveal disequilibrium of chloroplast phosphoglucose isomerase. *Plant, Cell and Environment* **22**: 525–533.

638 **Schmiege SC, Heskel M, Fan Y, Way DA**. **2023**. It's only natural: Plant respiration in unmanaged systems.
639 *Plant Physiology* **192**: 710–727.

Sharkey TD, Berry JA, Raschke K. **1985**. Starch and sucrose synthesis in *Phaseolus vulgaris* as affected by light, CO_2, and abscisic acid. *Plant Physiology* **77**: 617–620.

Sharkey TD, Weise SE. **2016**. The glucose 6-phosphate shunt around the Calvin–Benson cycle. *Journal of Experimental Botany* **67**: 4067–4077.

Stincone A, Prigione A, Cramer T, Wamelink MM, Campbell K, Cheung E, Olin-Sandoval V, Gruning N, Kruger A, Tauqeer Alam M, *et al.* 2015. The return of metabolism: biochemistry and physiology of the pentose phosphate pathway. *Biological Reviews Cambridge Philosphical Society* **90**: 927–963.

Szecowka M, Heise R, Tohge T, Nunes-Nesi A, Vosloh D, Huege J, Feil R, Lunn J, Nikoloski Z, Stitt M, *et al.* 2013. Metabolic fluxes in an illuminated *Arabidopsis* rosette. *The Plant Cell* **25**: 694–714.

Thalmann M, Santelia D. **2017**. Starch as a determinant of plant fitness under abiotic stress. *New Phytologist* **214**: 943–951.

Topper YJ. **1957**. On the mechanism of action of phosphoglucose isomerase and phosphomannose isomerase. *Journal of Biological Chemistry* **225**: 419–425.

Tsamir-Rimon M, Ben-Dor S, Feldmesser E, Oppenhimer-Shaanan Y, David-Schwartz R, Samach A, Klein T. **2021**. Rapid starch degradation in the wood of olive trees under heat and drought is permitted by three stress-specific beta amylases. *New Phytologist* **229**: 1398–1414.

Ubierna N, Holloway-Phillips M-M, Farquhar GD. **2022**. Scaling from fluxes to organic matter: interpreting ^{13}C isotope ratios of plant material using flux models. *New Phytologist* **236**: 2003–2008.

Vicente-Serrano SM, Beguería S, López-Moreno JI. **2010**. A multiscalar drought index sensitive to global warming: The standardized precipitation evapotranspiration index. *Journal of Climate* **23**: 1696–1718.

Wacker A. **2022**. Leaf sucrose shows no nighttime [2]H-depletion despite the degradation of strongly [2]H-depleted starch. Master thesis. University of Basel, Switzerland.

Wang X, Ruan M, Wan Q, He W, Yang L, Liu X, He L, Yan L, Bi Y. **2020**. Nitric oxide and hydrogen peroxide increase glucose-6-phosphate dehydrogenase activities and expression upon drought stress in soybean roots. *Plant Cell Reports* **39**: 63–73.

Wang H, Yang L, Li Y, Hou J, Huang J, Liang W. **2016**. Involvement of ABA- and H_2O_2-dependent cytosolic glucose-6-phosphate dehydrogenase in maintaining redox homeostasis in soybean roots under drought stress. *Plant Physiology and Biochemistry* **107**: 126–136.

Wendt UK, Wenderoth I, Tegeler A, Von Schaewen A. **2000**. Molecular characterization of a novel glucose-6-phosphate dehydrogenase from potato (*Solanum tuberosum* L.). *The Plant Journal* **23**: 723–733.

Wieloch T. **2021**. A cytosolic oxidation–reduction cycle in plant leaves. *Journal of Experimental Botany* **72**: 4186–4189.

Wieloch T. **2022**. High atmospheric CO_2 concentration causes increased respiration by the oxidative pentose phosphate pathway in chloroplasts. *New Phytologist* **235**: 1310–1314.

674   **Wieloch T, Augusti A, Schleucher J**. **2022a**. Anaplerotic flux into the Calvin-Benson cycle. Hydrogen
675   isotope evidence for *in vivo* occurrence in C$_3$ metabolism. *New Phytologist* **234**: 405–411.

676   **Wieloch T, Augusti A, Schleucher J**. **2023**. A model of photosynthetic CO$_2$ assimilation in C$_3$ leaves
677   accounting for respiration and energy recycling by the plastidial oxidative pentose phosphate pathway. *New*
678   *Phytologist* **239**: 518–532.

679   **Wieloch T, Ehlers I, Yu J, Frank D, Grabner M, Gessler A, Schleucher J**. **2018**. Intramolecular [13]C
680   analysis of tree rings provides multiple plant ecophysiology signals covering decades. *Scientific Reports* **8**:
681   5048.

682   **Wieloch T, Grabner M, Augusti A, Serk H, Ehlers I, Yu J, Schleucher J**. **2022b**. Metabolism is a major
683   driver of hydrogen isotope fractionation recorded in tree-ring glucose of *Pinus nigra*. *New Phytologist* **234**:
684   449–461.

685   **Wieloch T, Sharkey TD, Werner RA, Schleucher J**. **2022c**. Intramolecular carbon isotope signals reflect
686   metabolite allocation in plants. *Journal of Experimental Botany* **73**: 2558–2575.

687   **Wieloch T, Werner RA, Schleucher J**. **2021**. Carbon flux around leaf-cytosolic glyceraldehyde-3-
688   phosphate dehydrogenase introduces a ^{13}C signal in plant glucose. *Journal of Experimental Botany* **72**:
689   7136–7144.

690   **Supporting information**

691   Notes S1. Materials and Methods (expanded).

692   Notes S2. Hydro-carbon isotope fractionation during 1961 to 1980.

693   Notes S3. Estimated deuterium fractionation due to shifts of the phosphoglucose isomerase reaction.

694   Table S1. Shapiro-Wilk normality test.

695   Table S2. F and T test.

696   Table S3. Pearson correlations between $Δ_i$' and $ε_{met}$ series of the period 1983 to 1995.

697   Table S4. Components of variance in $Δ_i$ series.

698   Table S5. Pearson correlation coefficients and associated levels of significance of $ε_{met}$-climate relationships
699   for the period 1983 to 1995.

700   Table S6. Linear regression model of $ε_{met\ (H1)}$ as function of growing season air vapour pressure deficit and
701   March to July precipitation.

702   Figure S1. Air vapour pressure deficit of the growing season and March to July precipitation over the period
703   1961 to 1995 in the Vienna basin.

704

Table 1. Abbreviations and symbols.

Abbreviation	Definition
^{13}C signal	systematic $^{13}C/^{12}C$ variation
DAHPS	3-deoxy-D-arabino-heptulosonate 7-phosphate synthase
F6P	fructose 6-phosphate
G6P	glucose 6-phosphate
G6PD	glucose-6-phosphate dehydrogenase
GAP	glyceraldehyde 3-phosphate
GAPDH	glyceraldehyde-3-phosphate dehydrogenases
NMRS	nuclear magnetic resonance spectroscopy
OPPP	oxidative branch of the pentose phosphate pathway
PEP	phospho*enol*pyruvate
PEPC	phospho*enol*pyruvate carboxylase
PGA	3-phosphoglycerate
PGI	phosphoglucose isomerase
PK	pyruvate kinase
RuBP	ribulose 1,5-bisphosphate
TCAC	tricarboxylic acid cycle

Symbol	Definition
p_a	ambient CO_2 partial pressure
p_i	intercellular CO_2 partial pressure
PRE	precipitation
RAD	global radiation
SD	sunshine duration
$SPEI_i$	standardised precipitation-evapotranspiration index calculated for different timescales, $i = 1, 3, 6, 8, 12, 16, 24, 36, 48$ months
TMP	air temperature
VPD	air vapour pressure deficit
Δ	^{13}C discrimination denoting $^{13}C/^{12}C$ variation due to plant physiological processes
Δ_i'	intramolecular ^{13}C discrimination where i denotes individual glucose carbon positions and the prime denotes data corrected for ^{13}C signal redistribution by heterotrophic triose phosphate cycling
Δ_{1-2}'	arithmetic average of Δ_1' and Δ_2'
Δ_{1-3}'	arithmetic average of Δ_1', Δ_2', and Δ_3'
Δ_{5-6}'	arithmetic average of Δ_5' and Δ_6'
ε_{met}	metabolic deuterium fractionation at glucose H^1 and H^2

706

Table 2. Hydrogen isotope effects of phosphoglucose isomerase (PGI, Rose & O'Connell, 1961), and carbon isotope effects of glucose isomerase (GI, Gilbert *et al.*, 2012).

PGI, $\alpha = k_H/k_D$			GI, $\alpha = k_{12C}/k_{13C}$				
F6P, H[1R]		**G6P, H[2]**	**F6P, C-1**	**F6P, C-2**		**G6P, C-1**	**G6P, C-2**
	→	$2.\overline{2}$			→	1.005	1.015
0.9	↔	$1.\overline{1}$	1.013	0.993	↔	0.987	1.007
2	←		1.018	1.008	←		

→ kinetic isotope effect, ↔ equilibrium isotope effect. Calculated values underlined. Since GI and PGI have the same reaction mechanism, the ^{13}C isotope effects of GI and PGI are thought to be very similar (Gilbert *et al.*, 2012). H[1R], *pro-R* hydrogen at F6P C-1.

Table 3. Significance of Pearson correlations among Δ_1', Δ_2', and Δ_3' and climate series for the period 1983 to 1995 (n = 13).

Period / Δ_i'	VPD 1	2	3	PRE 1	2	3	$SPEI_1$ 1	2	3	$SPEI_3$ 1	2	3	$SPEI_4$ 1	2	3	$SPEI_6$ 1	2	3	$SPEI_8$ 1	2	3	$SPEI_{12}$ 1	2	3	$SPEI_{16}$ 1	2	3	$SPEI_{24}$ 1	2	3	$SPEI_{36}$ 1	2	3	$SPEI_{48}$ 1	2	3	TMP 1	2	3	SD 1	2	3	RAD 1	2	3
MAMJ	_c_	_a_	_b_		a		b		a	b		a	a																									_a_								_a_
MAMJJ	_c_		_b_	a	a	a	b		b	b		a	b		a	a						a																								
MAMJJA	_c_		_b_	b	a	a	c		b	c		b	b		a	b						a															_a_								
MAMJJAS	_c_		_b_	b	b		b		a	c		b	c		a	b		a	b																										_a_
MAMJJASO	_c_		_b_	a	a		b		a	c		a	c		a	b		a	b			a	a																						_a_
MAMJJASON	_c_		_b_	a	a		b		a	b		a	c		a	b		a	b			a	a																	_a_					_a_
AMJJ	_c_		_c_	a	a	a	a		b	b		b	b		b	b		a	a																							_a_			
AMJJA	_c_		_c_	a	a	a	b		b	c		b	c		b	b		a	b		a																_a_					_a_			
AMJJAS	_c_		_b_	a	b	a	b		b	c		b	c		b	b		a	b		a	a																							_a_
AMJJASO	_c_		_b_	a	a		b		a	c		b	c		b	c		b	b		a	a		a																		_a_			_a_
AMJJASON	_c_		_b_	a	b		a		a	b		a	c		b	c		a	c		a	b		a																_a_					_a_
MJJA	_b_		_b_	a			b		a	b		b	b		b	b		b	b		a	a		a													_a_		_a_						_a_
MJJAS	_b_		_b_	b	a	a	b		a	c		b	c		b	c		b	b		a	b		a																_a_					_a_
MJJASO	_c_		_b_	a			b		a	c		b	c		b	c		b	c		a	b		a																_a_					_a_
MJJASON	_c_		_b_	a	a		a		a	b		a	c		b	c		b	c		a	b		a																_a_					_a_
JJAS	_b_		_b_				a			b		b	b		b	c		b	b		a	b		a																					
JJASO	_b_		_b_							b		a	b		b	c		b	c		a	b		a																					
JJASON	_b_	_a_								b		a	b		a	b		b	c		b	b		a	a		a	a		a															
JASO	_a_	_a_								b		a	b		a	c		b	c		b	b		a	a		a	a		a						a									
JASON	_a_	_a_								a			b		a	b		b	c		b	b		a	a		a	a		a						a									
ASON	_c_	_a_											a			b		a	c		b	b		a	a		a	a		a						a				_b_					

Significance levels: ≤ 0.05, a; ≤ 0.01, b; ≤ 0.001, c. Underscore denotes negative correlation. Climate parameters: *PRE*, precipitation; *RAD*, global radiation; *SD*, sunshine duration; *SPEI*$_i$, standardised precipitation-evapotranspiration index of different periods (i = 1, 3, 6, 8, 12, 16, 24, 36, 48 months); *TMP*, air temperature; *VPD*, air vapour pressure deficit. Climate data were averaged for all ≥ 4-month periods of the growing season (March to November). Months were abbreviated by their initial letters. Δ_1', Δ_2', and Δ_3' denote intramolecular ^{13}C discrimination at glucose C-1, C-2, and C-3, respectively. Glucose was extracted across an annually resolved tree-ring series of *Pinus nigra*.

715 **Table 4: Linear regression models of Δ_1' and Δ_2', Δ_3' as function of ε_{met}, growing season**

720 **air vapour pressure deficit (*VPD*) and March to July precipitation (*PRE*).**

M1: Δ_1' ~ ε_{met} + *VPD*, 1983-1995		
R^2 = 0.87, $adjR^2$ = 0.84, $p < 10^{-4}$, n = 13		
Estimate	**± SE**	***p*** **≤**
Intercept 36.0	2.7	10^{-7}
ε_{met} -0.0187	0.0057	0.01
VPD -0.0295	0.0047	10^{-4}

M2: Δ_2' ~ ε_{met} + *VPD*, 1983-1995		
R^2 = 0.62, $adjR^2$ = 0.54, $p < 0.008$, n = 13		
Estimate	**± SE**	***p*** **≤**
Intercept 17.6	4.5	0.003
ε_{met} -0.0315	0.0097	0.009
VPD -0.0111	0.0080	0.2

M3: Δ_3' ~ ε_{met} + *VPD*, 1983-1995		
R^2 = 0.64, $adjR^2$ = 0.57, $p < 0.006$, n = 13		
Estimate	**± SE**	***p*** **≤**
Intercept 14.5	2.1	10^{-4}
ε_{met} -0.00615	0.00449	0.2
VPD -0.0129	0.0037	0.006

M4: Δ_2' ~ ε_{met}, 1983-1995		
R^2 = 0.54, $adjR^2$ = 0.50, $p < 0.004$, n = 13		
Estimate	**± SE**	***p*** **≤**
Intercept 11.8	1.7	10^{-4}
ε_{met} -0.0351	0.0097	0.004

M5: Δ_3' ~ *VPD*, 1983-1995		
R^2 = 0.57, $adjR^2$ = 0.53, $p < 0.003$, n = 13		
Estimate	**± SE**	***p*** **≤**
Intercept 14.3	2.2	10^{-4}
VPD -0.0143	0.0037	0.003

M6: Δ_1' ~ *PRE* + *VPD*, 1983-1995		
R^2 = 0.82, $adjR^2$ = 0.79, $p < 0.001$, n = 13		
Estimate	**± SE**	***p*** **≤**
Intercept 27.8	4.4	10^{-4}
PRE 0.0146	0.0061	0.04
VPD -0.0280	0.0058	0.001

M7: Δ_2' ~ *PRE*, 1983-1995		
R^2 = 0.43, $adjR^2$ = 0.37, $p < 0.02$, n = 13		
Estimate	**± SE**	***p*** **≤**
Intercept -1.84	2.79	0.52
PRE 0.0274	0.0096	0.016

M8: Δ_3' ~ *VPD*, 1961-1980		
R^2 = 0.13, $adjR^2$ = 0.07, $p = 0.15$, n = 18		
Estimate	**± SE**	***p*** **≤**
Intercept 12.3	3.8	0.006
VPD -0.0112	0.0074	0.15

M9: Δ_1' ~ *PRE* + *VPD*, 1961-1980		
R^2 = 0.07, $adjR^2$ = 0, $p > 0.55$, n = 18		

24

	Estimate	± SE	p ≤
Intercept	18.6	4.8	0.002
PRE	0.00273	0.00407	0.51
VPD	-0.00357	0.00781	0.65

M10: Δ_2' ~ *PRE*, 1961-1980		
$R^2 = 0.05$, $adjR^2 = 0$, $p = 0.35$, $n = 18$		

	Estimate	± SE	p ≤
Intercept	6.92	0.93	10^{-5}
PRE	0.00276	0.00286	0.35

M11: ε_{met} ~ *PRE* + *VPD*, 1983-1995		
$R^2 = 0.71$, $adjR^2 = 0.66$, $p < 0.002$, $n = 13$		

	Estimate	± SE	p ≤
Intercept	437	118	0.004
PRE	-0.777	0.164	0.001
VPD	-0.082	0.155	0.61

721   ε_{met}, Δ_1', Δ_2', and Δ_3' denote hydrogen isotope fractionation caused by metabolic processes at

722   glucose H^1 and H^2, and carbon isotope discrimination at glucose C-1, C-2, and C-3, respectively.

723   Glucose was extracted across an annually resolved tree-ring series of *Pinus nigra* from the Vienna

724   Basin.

725

Table 5. Significance of Pearson correlations among $Δ_1'$, $Δ_2'$, and $Δ_3'$ and climate series for the period 1961 to 1980 (n = 18).

Period / $Δ_i'$	VPD			PRE			$SPEI_1$			$SPEI_3$			$SPEI_4$			$SPEI_6$			$SPEI_8$			$SPEI_{12}$			$SPEI_{16}$			$SPEI_{24}$			$SPEI_{36}$			$SPEI_{48}$			TMP			SD			RAD		
	1	2	3	1	2	3	1	2	3	1	2	3	1	2	3	1	2	3	1	2	3	1	2	3	1	2	3	1	2	3	1	2	3	1	2	3	1	2	3	1	2	3	1	2	3
MAMJ	<u>a</u>						a			a			a											a			a													<u>a</u>			<u>a</u>		
MAMJJ										a														a			a																		
MAMJJA																								a			a																		
MAMJJAS						a																		a			b		a																
MAMJJASO							a																	a			b		a																
MAMJJASON																								a			b		a																
AMJJ										a			a											a			b																		
AMJJA						a																		a			b																		
AMJJAS						b			a															a			b		a																
AMJJASO						a																		a			b		a																
AMJJASON						a																		a			b		a																
MJJA					a	a																		a			b		a																
MJJAS					a	b			a															a			b		a																
MJJASO						a																					b		a																
MJJASON						a																					b		a																
JJAS					a	b			a																		b		a			a													
JJASO																											b		a			a													
JJASON																											b		a			a													
JASO		<u>a</u>																									b		a			a													
JASON								<u>a</u>																			b		a			a													
ASON		<u>a</u>																									b		a			a													

Significance levels: ≤ 0.05, a; ≤ 0.01. Underscore denotes negative correlation. Climate parameters: *PRE*, precipitation; *RAD*, global radiation; *SD*, sunshine duration; *SPEI*$_i$, standardised precipitation-evapotranspiration index of different periods (i = 1, 3, 6, 8, 12, 16, 24, 36, 48 months); *TMP*, air temperature; *VPD*, air vapour pressure deficit. Climate data were averaged for all ≥ 4-month periods of the growing season (March to November). Months were abbreviated by their initial letters. $Δ_1'$, $Δ_2'$, and $Δ_3'$ denote intramolecular ^{13}C discrimination at glucose C-1, C-2, and C-3, respectively. Glucose was extracted across an annually resolved tree-ring series of *Pinus nigra*.

Table 6. Significance of Pearson correlations among Δ_4', Δ_5', and Δ_6' and climate series for the period 1961 to 1995 (n = 31).

Period / Δ_i'	VPD 4	VPD 5	VPD 6	PRE 4	PRE 5	PRE 6	$SPEI_1$ 4	$SPEI_1$ 5	$SPEI_1$ 6	$SPEI_3$ 4	$SPEI_3$ 5	$SPEI_3$ 6	$SPEI_4$ 4	$SPEI_4$ 5	$SPEI_4$ 6	$SPEI_6$ 4	$SPEI_6$ 5	$SPEI_6$ 6	$SPEI_8$ 4	$SPEI_8$ 5	$SPEI_8$ 6	$SPEI_{12}$ 4	$SPEI_{12}$ 5	$SPEI_{12}$ 6	$SPEI_{16}$ 4	$SPEI_{16}$ 5	$SPEI_{16}$ 6	$SPEI_{24}$ 4	$SPEI_{24}$ 5	$SPEI_{24}$ 6	$SPEI_{36}$ 4	$SPEI_{36}$ 5	$SPEI_{36}$ 6	$SPEI_{48}$ 4	$SPEI_{48}$ 5	$SPEI_{48}$ 6	TMP 4	TMP 5	TMP 6	SD 4	SD 5	SD 6	RAD 4	RAD 5	RAD 6
MAMJ																						<u>a</u>			<u>a</u>																<u>b</u>			<u>b</u>	
MAMJJ		<u>a</u>			a			a			a											<u>a</u>			<u>a</u>																<u>b</u>			<u>b</u>	a
MAMJJA		<u>a</u>			a			a			a			a																											<u>b</u>			b	b
MAMJJAS		<u>a</u>									a			a		a																									<u>b</u>			b	b
MAMJJASO											a			a		a			a																						<u>a</u>			b	b
MAMJJASON		<u>a</u>												a		a			a																						<u>a</u>			b	b
AMJJ	<u>b</u>	a		b			c	a		b			a												<u>a</u>												a	<u>a</u>	a	<u>c</u>			c	a	
AMJJA	<u>b</u>	a		b			b	a		b			b			a			a																			<u>a</u>	a	<u>c</u>	a		c	b	
AMJJAS	a	<u>a</u>		a			b	a		b			b			a			a																				a	<u>c</u>	a		c	c	
AMJJASO	a	<u>a</u>		a			b	a		a			b			b			a																				a	<u>b</u>			c	c	
AMJJASON	a	<u>a</u>					a	a		a			a			a			a																				a	<u>b</u>			c	c	
MJJA	<u>b</u>	a		a	a		b	a		c	a		b			b			a																			<u>a</u>	b	<u>c</u>	a		c	b	
MJJAS	a	<u>a</u>		a	a		b	a		b	a		b	a		b			a																			<u>a</u>	b	<u>b</u>	a		b	c	
MJJASO	a	<u>a</u>		a	a		b	a		b	a		b	a		b	a		a				a																a	<u>b</u>			b	c	
MJJASON	a	<u>a</u>					a	a		a	a		b	a		b	a		b				a															<u>a</u>	b	<u>a</u>			b	c	
JJAS	a	<u>a</u>								b	a		b	a		b			a				a																		<u>b</u>		a		c
JJASO		<u>a</u>								b	a		b	a		b	a		a				a																		<u>a</u>				c
JJASON	a	<u>a</u>								a	a		a	a		b	a		b				a																		<u>a</u>		a		c
JASO		<u>a</u>								a	a		b	a		b	a		b				a												a										b
JASON		<u>a</u>									a		a	a		b	a		b	a			a																			<u>a</u>				b
ASON				<u>a</u>												b	a		a				a																						b

Significance levels: ≤ 0.05, a; ≤ 0.01, b; ≤ 0.001, c. Underscore denotes negative correlation. Climate parameters: *PRE*, precipitation; *RAD*, global radiation; *SD*, sunshine duration; *SPEI_i*, standardised precipitation-evapotranspiration index of different periods (i = 1, 3, 6, 8, 12, 16, 24, 36, 48 months); *TMP*, air temperature; *VPD*, air vapour pressure deficit. Climate data were averaged for all ≥ 4-month periods of the growing season (March to November). Months were abbreviated by their initial letters. Δ_4', Δ_5', and Δ_6' denote intramolecular ^{13}C discrimination at glucose C-4, C-5, and C-6, respectively. Glucose was extracted across an annually resolved tree-ring series of *Pinus nigra*.

739 **Table 7: Linear regression models of Δ_4', Δ_5', and Δ_6' as function of April to September global**

740 **radiation (RAD), and March to October air temperature (TMP).**

M1: $\Delta_{5\text{-}6}$' ~ RAD + TMP, 1964-1995		
$R^2 = 0.72$, $adjR^2 = 0.70$, $p = 10^{-7}$, $n = 28$		
	Estimate	**± SE**	**$p \le$**
Intercept	26.0	3.1	10^{-8}
RAD	-0.00843	0.00105	10^{-7}
TMP	1.35	0.29	10^{-4}
M2: Δ_5' ~ RAD + TMP, 1964-1995		
$R^2 = 0.66$, $adjR^2 = 0.64$, $p = 10^{-6}$, $n = 28$		
	Estimate	**± SE**	**$p \le$**
Intercept	24.8	4.3	10^{-5}
RAD	-0.0103	0.0015	10^{-6}
TMP	1.81	0.40	10^{-4}
M3: Δ_6' ~ RAD + TMP, 1964-1995		
$R^2 = 0.47$, $adjR^2 = 0.43$, $p < 0.001$, $n = 28$		
	Estimate	**± SE**	**$p \le$**
Intercept	27.3	4.2	10^{-6}
RAD	-0.00658	0.00144	10^{-4}
TMP	0.876	0.393	0.04
M4: $\Delta_{5\text{-}6}$' ~ RAD + TMP, 1964-1980		
$R^2 = 0.69$, $adjR^2 = 0.63$, $p < 0.001$, $n = 15$		
	Estimate	**± SE**	**$p \le$**
Intercept	31.2	6.7	0.001
RAD	-0.00906	0.00177	0.001
TMP	1.11	0.47	0.04
M5: $\Delta_{5\text{-}6}$' ~ RAD + TMP, 1983-1995		
$R^2 = 0.82$, $adjR^2 = 0.79$, $p < 0.001$, $n = 13$		
	Estimate	**± SE**	**$p \le$**
Intercept	29.1	4.5	10^{-4}
RAD	-0.00875	0.00132	10^{-4}
TMP	1.22	0.40	0.01
M6: Δ_4' ~ RAD + TMP, 1964-1995		
$R^2 = 0.15$, $adjR^2 = 0.09$, $p = 0.12$, $n = 28$		
	Estimate	**± SE**	**$p \le$**
Intercept	8.33	4.73	0.09
RAD	-0.00266	0.00160	0.11
TMP	0.931	0.439	0.04

741 Δ_4', Δ_5', and Δ_6' denote carbon isotope discrimination at glucose C-4, C-5, and C-6, respectively.

742 Glucose was extracted across an annually resolved tree-ring series of *Pinus nigra* from the Vienna
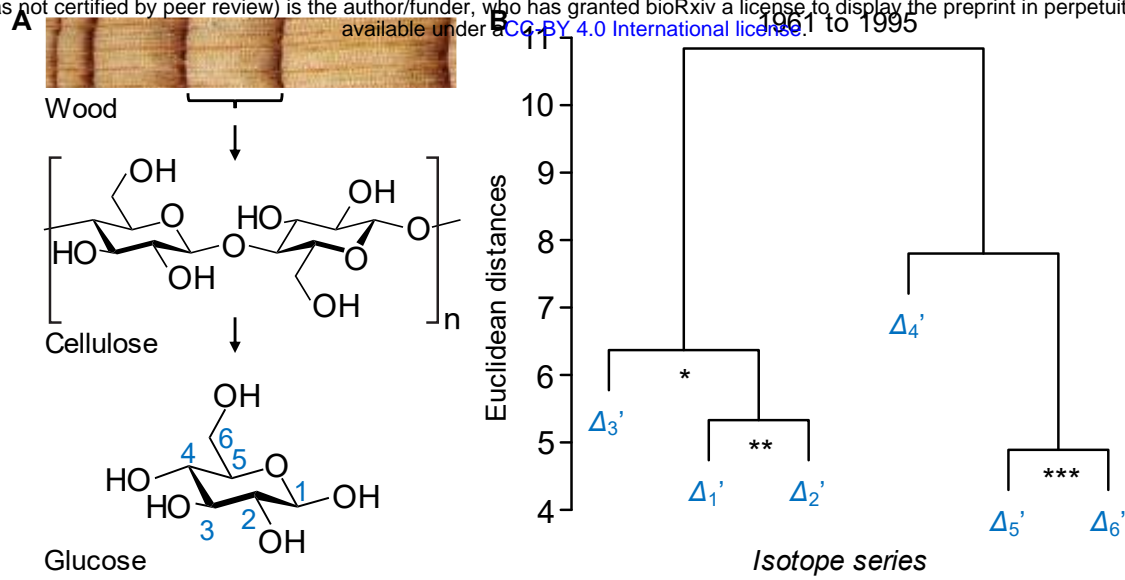
743 Basin.

744

28

Figure 1. Carbon isotope discrimination in tree rings. (A) Levels of resolution of stable carbon isotope analysis: whole plant materials, whole molecules, intramolecular carbon positions. **(B)** Hierarchical clustering of Δ_i' series for the period 1961 to 1995. Significance of series correlation: *, $p \leq 0.05$; **, $p \leq 0.01$; ***, $p \leq 0.001$. Modified figure from Wieloch *et al.* (2018). Δ_i' denotes intramolecular ^{13}C discrimination in glucose extracted across an annually resolved *Pinus nigra* tree-ring series.

Figure 2. Proposed metabolic origins of carbon and hydrogen isotope signals in tree-ring glucose. Dashed arrows indicate that intermediate reactions are not shown. Abbreviations: 2PG, 2-phosphoglycolate; 2PGA, 2-phosphoglycerate; 6PGL, 6-phosphogluconolactone; ADP, adenosine diphosphate; ATP, adenosine triphosphate; CIT, citrate; COR cycle, cytosolic oxidation-reduction cycle; DAHP, 3-Deoxy-D-*arabino*-heptulosonate 7-phosphate; DAHPS, DAHP synthase; E4P, erythrose 4-phosphate; F6P, fructose 6-phosphate; FAD, flavin adenine dinucleotide; Fru, fructose; G6P, glucose 6-phosphate; G6PD, G6P dehydrogenase; GDC, glycine decarboxylase complex; Glc, glucose; MEP pathway, methylerythritol 4-phosphate pathway; NAD^+, nicotinamide adenine dinucleotide; $NADP^+$, nicotinamide adenine dinucleotide phosphate; np-GAPDH, non-phosphorylating glyceraldehyde-3-phosphate dehydrogenase; OAA, oxaloacetate; OPPP, oxidative pentose phosphate pathway; PEP, phospho*enol*pyruvate; PEPC, PEP carboxylase; p-GAPDH, phosphorylating glyceraldehyde-3-phosphate dehydrogenase; PGA, 3-phosphoglycerate; PGI, phosphoglucose isomerase; PGK, phosphoglycerate kinase; P_i, inorganic phosphate; PK, pyruvate kinase; PP, pentose phosphate; *PRE*, precipitation; Pyr, pyruvate; Rubisco, ribulose-1,5-bisphosphate carboxylase/oxygenase; RuBP, ribulose 1,5-bisphosphate; *RAD*, global radiation; Suc, sucrose; SuSy, sucrose synthase; TCAC, tricarboxylic acid cycle; TK, transketolase; *TMP*, air temperature; TP, triose phosphates (glyceraldehyde 3-phosphate, dihydroxyacetone phosphate); UDPG, uridine diphosphate glucose; *VPD*, air vapour pressure deficit; Δ_i', intramolecular ^{13}C discrimination where *i* denotes individual glucose carbon positions and the prime denotes data corrected for ^{13}C signal redistribution by heterotrophic triose phosphate cycling; ε_{met}, metabolic deuterium fractionation at glucose H^1 and H^2.

A

$\Delta_1' = -0.028\varepsilon_{met} + ...$
$R^2 = 0.35$
$p = 0.03$

B

$\Delta_2' = -0.035\varepsilon_{met} + 11.84$
$R^2 = 0.54$
$p = 0.004$

C

$\Delta_3' = -0.010\varepsilon_{met} + 7.74$
$R^2 = 0.21$
$p = 0.12$

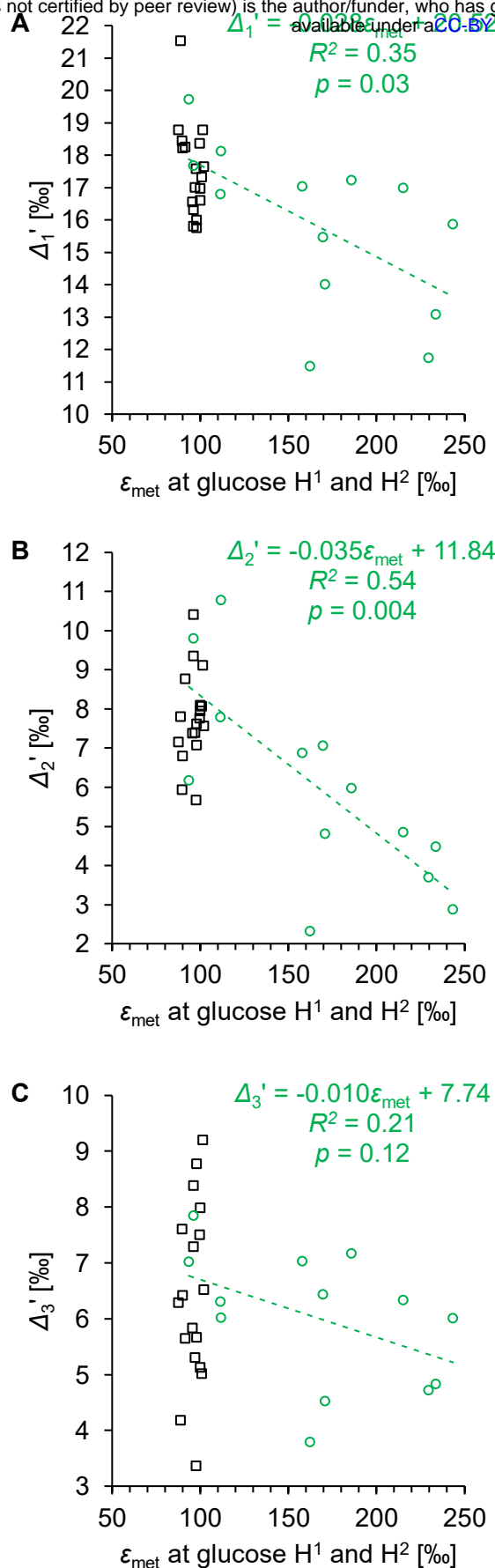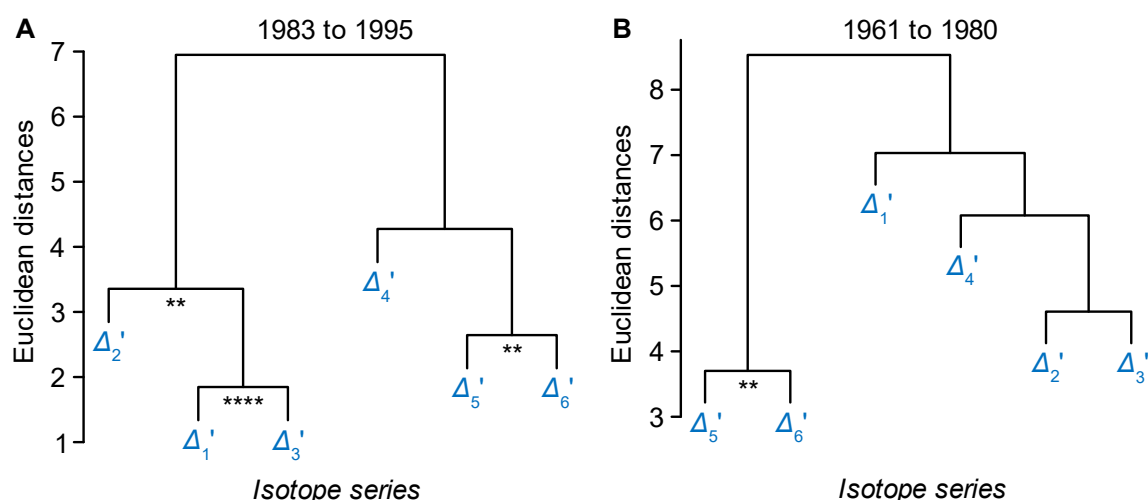**Figure 3. Relationship between the average hydrogen isotope fractionation caused by metabolic processes at glucose H^1 and H^2 (ε_{met}) and ^{13}C discrimination at C-1, C-2, and C-3 (Δ_1', Δ_2', and Δ_3').** Glucose was extracted across an annually resolved tree-ring series of *Pinus*

775   *nigra* from the Vienna Basin (black squares; 1961 to 1980; green circles; 1983 to 1995). Dashed

780   line, relationship between the hydrogen and carbon isotope data of the period 1983 to 1995.

781

782

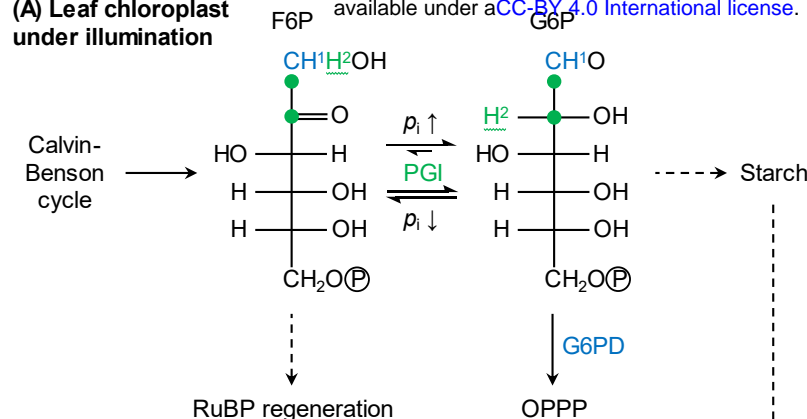**Figure 4. Hierarchical clustering of Δ_i' series for the periods 1983 to 1995 (A) and 1961 to 1980 (B).** Δ_i denotes intramolecular ^{13}C discrimination in tree-ring glucose of *Pinus nigra* from the Vienna basin with *i* denoting individual glucose carbon positions. Significance of series correlation: **, $p \leq 0.01$; ****, $p \leq 10^{-4}$.
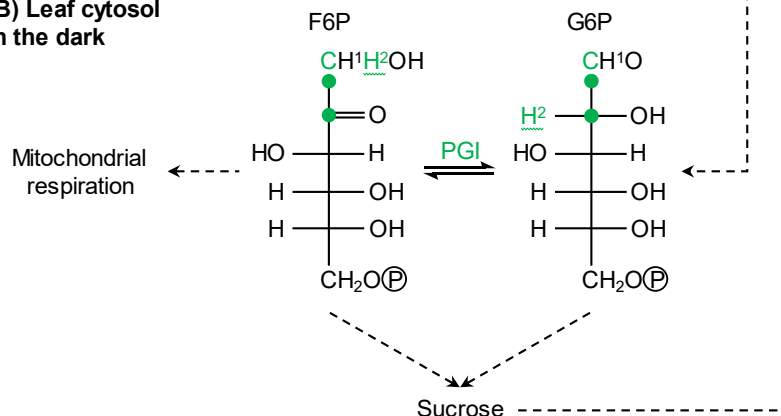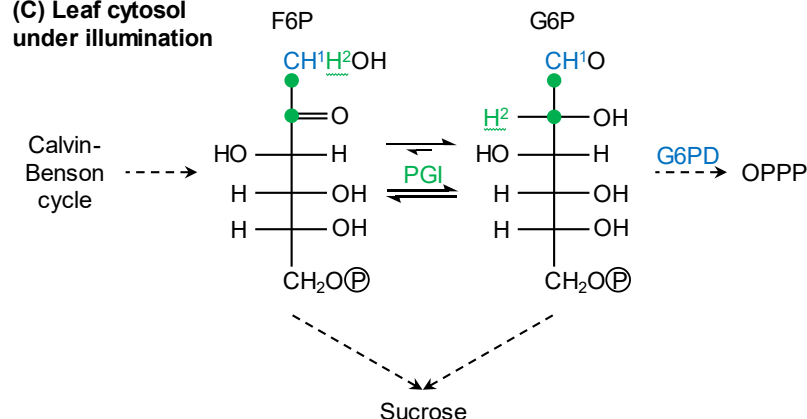
787

33

(A) Leaf chloroplast under illumination

F6P

G6P

CH^{1}H^{2}OH

CH^{1}O

Calvin-Benson cycle

$p_i \uparrow$

PGI

$p_i \downarrow$

HO——H

H——OH

H——OH

CH$_2$O℗

HO——H

H——OH

H——OH

CH$_2$O℗

H^2——OH

Starch

G6PD

RuBP regeneration

OPPP

(B) Leaf cytosol in the dark

F6P

G6P

CH^{1}H^{2}OH

CH^{1}O

PGI

HO——H

H——OH

H——OH

CH$_2$O℗

HO——H

H——OH

H——OH

CH$_2$O℗

H^2——OH

Mitochondrial respiration

Sucrose

(C) Leaf cytosol under illumination

F6P

G6P

CH^{1}H^{2}OH

CH^{1}O

Calvin-Benson cycle

PGI

HO——H

H——OH

H——OH

CH$_2$O℗

HO——H

H——OH

H——OH

CH$_2$O℗

H^2——OH

G6PD

OPPP

Sucrose

(D) Stem cytosol

Sucrose

Sucrose

Leucoplast starch

F6P

G6P

CH^{1}H^{2}OH

CH^{1}O

$PRE \downarrow$

PGI

$PRE \uparrow$

HO——H

H——OH

H——OH

CH$_2$O℗

HO——H

H——OH

H——OH

CH$_2$O℗

H^2——OH

Tree-ring glucose

G6PD
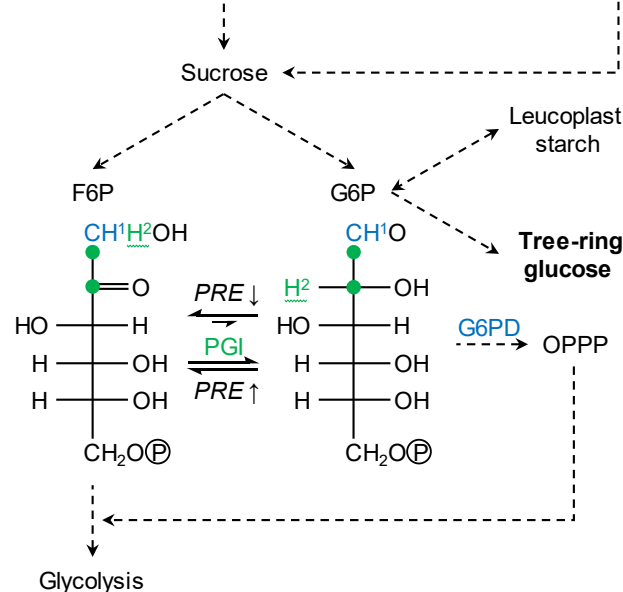
OPPP

Glycolysis

788

789 **Figure 5. Processes invoked to explain isotope fractionation at tree-ring glucose HC-1 and**

790 **HC-2: (A) in leaf chloroplasts under illumination, (B) in the leaf cytosol in the dark, (C) in the**

791 **leaf cytosol under illumination, and (D) in the stem cytosol.** F6P and G6P carbon atoms 1 to 6

792 occur in sequentially order from top to bottom. Atom positions affected by G6PD and PGI

793 fractionation are given in blue and green, respectively. In some cases, carbon position 1 is given

794 both as blue letter and green dot to indicate fractionation at both enzymes. Dashed arrows indicate

795 that intermediate reactions are not shown. Wavy lines indicate fractional introduction of hydrogen

796 from water by the PGI reaction. Note, G6PD in stem leucoplasts may additionally contribute to

797 isotope fractionation at tree-ring glucose C-1 and H[1]. Abbreviations: F6P, fructose 6-phosphate;

798 G6P, glucose 6-phosphate; G6PD, G6P dehydrogenase; OPPP, oxidative pentose phosphate

799 pathway; p_i, intercellular CO_2 partial pressure; PGI, phosphoglucose isomerase; *PRE*; precipitation;
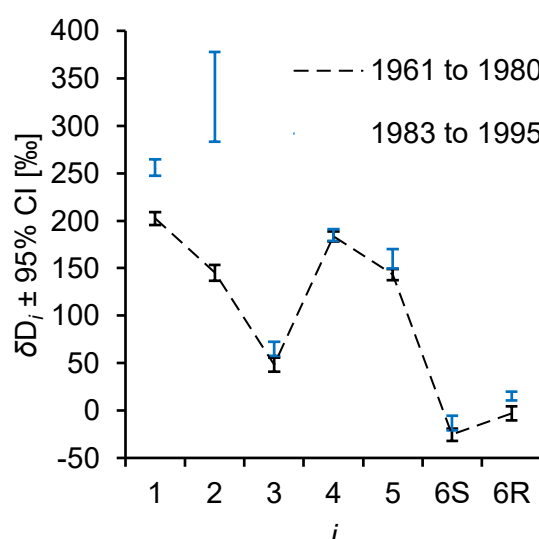
800 RuBP, ribulose 1,5-bisphosphate.

801

802

803 **Figure 6. Average intramolecular δD_i patterns of the periods 1961 to 1980 and 1983 to 1995**

804 **(black and blue, respectively).** The data were acquired for tree-ring glucose of *Pinus nigra* laid

805 down at a site in the Vienna basin. The figure shows discrete data. Dashed and dotted lines were

806 added to guide the eye. Data reference: Average deuterium abundance of the methyl-group

807 hydrogens of the glucose derivative used for NMRS measurements. Modified figure from Wieloch

808 *et al.* (2022b).

809